Regulation of excitatory presynaptic activity by Ambra1 protein determines neuronal networks in sex-dimorphic manner

Anes Ju[1,2#], Bekir Altas[1], Hong Jun Rhee[1], Manuela Schwark[1], Imam Hassouna[2], Albrecht Sigler[1], Hiroshi Kawabe[1], Kamal Chowdhury[3], Hannelore Ehrenreich[2], Nils Brose[1] and JeongSeop Rhee[1]*

[1]Department of Molecular Neurobiology, Max Planck Institute for Multidisciplinary Sciences (City Campus), Göttingen, Germany

[2]Clinical Neuroscience, Max Planck Institute for Multidisciplinary Sciences (City Campus), Göttingen, Germany

[3]Department of Molecular Cell Biology, Max Planck Institute for Multidisciplinary Sciences (Faßberg Campus), Göttingen, Germany

[#]Current address: Samsung Advanced Institute of Technology, Samsung Electronics, Suwon-si, South Korea

*Correspondence: rhee@mpinat.mpg.de

Abstract

Heterozygous mutation of *Ambra1*, known as a positive autophagy regulator, produces autism-like behavior in mice and autistic phenotypes in humans in a female-specific manner. However, the substantial roles of the *Ambra1* mutation in neurons are still unknown. We find that *Ambra1* heterozygotes display a moderate decrease in excitatory synaptic release *in-vitro* and *ex-vivo* exclusively in females without autophagy activity, resulting in significant alterations in γ-oscillation power and seizure susceptibility by excitatory/inhibitory (E/I) imbalance. Specifically, *Ambra1* deficiency has no effect on neurogenesis and morphogenesis, but selectively decreases excitatory synaptic activity without changes in synapse number, quantal size, synaptic release probability, and synaptic plasticity. Therefore, the limited excitatory synaptopathy by Ambra1 expression levels ultimately determines E/I imbalance in global neural networks leading to the female-specific ASD.

Keywords

Ambra1, E/I imbalance, Autism, Synaptic transmission, Seizure, Oscillations, Sex-dimorphism

Introduction

Autism-spectrum disorder (ASD) is a neurodevelopmental disorder mainly characterized by deficits in social interaction/communication and restricted/repetitive patterns of behavior (Association, 2013). Epidemiological studies estimated that ASD has been diagnosed in more than 1% of the world's population (Elsabbagh et al., 2012; Vos et al., 2016) and described as a sexually-dimorphic disease, with four times more males than females being diagnosed (Baron-Cohen et al., 2011; Chakrabarti and Fombonne, 2001). Genetic etiology of ASD is highly heterogenous, with greater than 100 identified risk genes involved in diverse functions, such as transcriptional regulation, protein synthesis and degradation, synapse function and synaptic plasticity (Bourgeron, 2015; Delorme et al., 2013; Ebert and Greenberg, 2013). Whether genetically distinct forms of ASD share common pathophysiology at the neural network level still remains to be elucidated.

Emerging evidence has suggested a disturbed homeostasis of excitatory/inhibitory (E/I) balance as an etiology of ASD (Nelson and Valakh, 2015; Zikopoulos and Barbas, 2013). Epilepsy, relatively high comorbidity in ASD, occurring in 5-38% of autistic individuals, highlights the possibility of shared neurophysiological mechanisms involved with changed neural network activities ("Epilepsy and autism spectrum disorders may have a shared aetiology," 2016; Lee et al., 2015). This hypothesis is corroborated by electroencephalogram (EEG) abnormalities often observed in patients with ASD or epilepsy (Martinerie et al., 1998; Mathalon et al., 2015; Rossi et al., 1995; Spence and Schneider, 2009), addressing that altered neuronal network and synchronicity are related with those two diseases. Based on several mouse studies proposing sexually dimorphic mechanisms regulating neural circuits (Li et al., 2016; Malishkevich et al., 2015), E/I balance is a critical factor of ASD in a sexually-dimorphic manner. However, the neurophysiological substrates of E/I imbalance in ASD still stimulates our curiosity.

Ambra1 (activating molecule in Beclin1-regulated autophagy) is a crucial regulator in autophagy, proliferation and apoptosis in eukaryotic cells (Maria Fimia et al., 2007). Homozygous mutation of *Ambra1* gene in mice (*Ambra1*$^{gt/gt}$) resulted in embryonic lethality showing neural tube defects (Maria Fimia et al., 2007). Interestingly, *Ambra1* heterozygous mice (*Ambra1*$^{+/gt}$), that are viable, produced clear autism-like behaviors only in females, which might be linked to sexually-dimorphic expression of Ambra1 protein in brain tissue (Dere et al., 2014). Additionally, our previous study showed early brain enlargement and different seizure propensity depending on developmental stages in this mouse line in a female-specific manner supporting *Ambra1*$^{+/gt}$ mice as a model of female-specific ASD (Mitjans et al., 2017). Especially, this study includes human genetic research reporting a significant association between autistic

69 features and intronic single nucleotide polymorphisms of the *AMBRA1* gene in females but not
70 in males. Therefore, *Ambra1* heterozygous mice is proved as a construct-valid genetic mouse
71 model of female ASD (Mitjans et al., 2017).
72 The present study has been designed to explore the neural substrate underlying this E/I
73 balance observed in the brains of *Ambra1*$^{+/gt}$ females by screening functional and
74 morphological aspects of neural network in brain slice. In addition, in order to define the precise
75 role of the Ambra1 protein, we studied the functional consequences by the absence of *Ambra1*
76 gene in autaptic neuronal culture of *Ambra1* homozygous mutation. Our study revealed that
77 Ambra1 present in the brain was limitedly located in neuronal cells, and was particularly
78 accumulated in the synapses. We found that, regardless of sex, Ambra1 was directly involved
79 in excitatory synaptic activity, while showing no effect on neuronal development and synapse
80 formation. More importantly, it was noticed that the reduction of excitatory synaptic activity by
81 *Ambra1* heterozygosity only in females, although not significant, is a decisive cause of synaptic
82 E/I input imbalance, contributing to ASD.
83

84 ## Results

85 *Region-, cell type- and subcellular-specific expression of Ambra1 protein*
86 We first analyzed the expression pattern of Ambra1 protein in region, different cell types and
87 subcellular location of mouse brain. mRNA expression data from Allen brain atlas revealed
88 that *Ambra1* is widely present (Figure 1A). Histochemical or immunofluorescent staining of β-
89 galactosidase (β-gal) in mouse brains showed that Ambra1 is abundantly expressed in cortex,
90 striatum and hippocampus and in neurons, but not in glial cells (Figure 1B-E). Subcellular
91 fractionation of *Ambra1*$^{+/+}$ cortex (Figure 1F) (Bermejo et al., 2014), where the purification of
92 synaptic membrane was validated (Figure 1G), was used for Western Blot of Ambra1 protein.
93 Surprisingly, Ambra1 protein was identified not only in ER-Golgi enriched fractions (P2B) but
94 also in crude synaptic membrane (CSM) and pure synaptic membrane fractions (SM, Figure
95 1G). These data illustrate that Ambra1 protein is located only in neurons and is particularly
96 distributed in synapses, suggesting a possibility of its role in neuronal communication.
97

98 *No change in activity-dependent synaptic plasticity upon Ambra1 heterozygous mutation*
99 Due to neuronal expression and synaptic location of Ambra1 protein, we sought to determine
100 the consequences of *Ambra1* heterozygous mutation in neural networks for learning and
101 memory. Based on previous studies showing the modification of synaptic plasticity and
102 oscillatory activity in several ASD mouse models (Hammer et al., 2015; Mathalon et al., 2015),
103 we recorded them in acute hippocampal slices from 4 week-old mice before sexual maturation

104 (Heiniger H. J. and Dorey, 1989), using extracellular recording. Overall, we found the input-
105 output curve, paired-pulse ratio, and early-phase long-term potentiation (Figure 2) were
106 comparable between two genotypes in male and female mice, pointing out that, upon *Ambra1*
107 heterozygous mutation, activity-dependent synaptic activities and plasticity are unaltered.
108
109 *Perturbed γ-power and seizure propensity by Ambra1 heterozygous mutation only in females*
110 *but not in males*
111 To specifically and concretely measure the local activity of neural network, we assessed the
112 oscillatory activity in hippocampal CA3 pyramidal layer induced by Kainate. The peak
113 frequencies were detected within γ-range (25-45 Hz) and comparable between two genotypes.
114 Intriguingly, the average power of γ-oscillation was significantly lower in *Ambra1*$^{+/gt}$ females
115 compared to control littermates, while male mice exhibited similar levels between two
116 genotypes (Figure 3D-E), indicating female-specific alteration of synchrony of neural network
117 activities in *Ambra1*$^{+/gt}$ brains.
118 Epilepsy, one of the comorbid conditions of ASD (Bolton et al., 2011), is a behavioral feature
119 manifested by abnormal synchrony of neural network activities (Sun et al., 2021). The seizure
120 threshold was markedly higher in *Ambra1*$^{+/gt}$ females compared to control, which is shown by
121 earlier latency of whole-body seizure episodes and higher seizure score, whereas those
122 parameters were similar between two genotypes in males (Figure 3F-G). Taken together,
123 higher seizure propensity and lower power of gamma oscillations in heterozygous females
124 demonstrate that female mice are more sensitive to disturbed synchronous network activity
125 upon *Ambra1* heterozygous mutation.
126
127 *E/I imbalance by change in functional excitatory synapses, regardless of autophagy activity*
128 To investigate the cellular substrates underlying the E/I imbalance which is the significant
129 mechanism causing the abnormal synchronization in a neuronal network, we first compared
130 the population of excitatory and inhibitory neurons between two genotypes. The densities, sum
131 and ratio of the mature glutamatergic (CTIP2+) and GABAergic (GAD67+) neurons as well as
132 the density of parvalbumin-expressing (PV+) interneurons were similar in pyramidal layer of
133 hippocampus between *Ambra1*$^{+/+}$ and *Ambra1*$^{+/gt}$ female mice (Figure 4A-G). This data
134 suggests that the *Ambra1* heterozygous mutation is not crucial for neuronal proliferation and
135 apoptosis, which are not a main factor for the alteration in γ-oscillation power in this mouse
136 line.
137 By Western blotting with the anti-LC3 antibody, LC3-II/LC3-I ratio, an indicative of autophagic
138 activity, was similar between *Ambra1*$^{+/+}$ and *Ambra1*$^{+/gt}$ in female cortical homogenates (Figure
139 4H-I). This is corroborated by unaltered expression levels of different synaptic proteins in

140 hippocampal homogenates or cortical synaptosomal fractions between two genotypes (Figure
141 S1). Therefore, our data imply that the autophagic activity of Ambra1 unaccompanied by
142 neuron is not a critical factor in the E/I imbalance.
143 We measure miniature excitatory and inhibitory postsynaptic currents (mEPSC and mIPSC) at
144 the same neuron in acute brain slice and morphological features by simultaneously filling the
145 recorded neurons with biocytin, as a minimal functional model system (Figure 3A).
146 The morphological properties of hippocampal pyramidal neurons, including dendritic
147 arborization and number of mushroom spines (Figure 5A-C), were unaltered by *Ambra1*
148 heterozygous mutation, which is additionally supported by independent experiments using *in*
149 *utero* electroporated samples (Figure S2). Moreover, PSD95 and Gephyrin as well as
150 PSD95/Gephyrin expression, implying the number of excitatory and inhibitory post-synapses
151 and their ratio, were not altered in *Ambra1*$^{+/gt}$ brains (Figure S1C-D). Similar neuronal
152 morphology and expression levels of postsynaptic proteins can infer that the number of
153 excitatory and inhibitory postsynapses were unchanged by *Ambra1* heterozygous mutation.
154 Without changes in mEPSC and mIPSC amplitudes, only mEPSC frequencies of female
155 *Ambra1*$^{+/gt}$ neurons showed a strong tendency for reduction (Figure 5D-F), suggesting that the
156 possibility due to a decrease in the number of functional glutamatergic synapses cannot be
157 excluded. Surprisingly, the ratio of frequencies of mIPSC and mEPSC, which indirectly
158 described the cellular E/I balance, was significantly increased in *Ambra1*$^{+/gt}$ females compared
159 to control littermates, while male mice showed a similar trend without significance (Figure 5E).
160 These data indicate that the ratio of excitatory and inhibitory inputs into single cells can be a
161 critical factor in network homeostasis (Huang et al., 2021; Xue et al., 2014) rather than the
162 change in the number of overall inputs themselves.
163 Subtle phenotypes of synaptic function by *Ambra1* heterozygous mutation lead to further
164 analysis of synaptic release by the absence of *Ambra1* gene. We accessed the synaptic
165 release property of glutamatergic autaptic neurons cultured from cortex of *Ambra1*$^{+/+}$,
166 *Ambra1*$^{+/gt}$ and *Ambra1*$^{gt/gt}$ embryonic littermate in both sexes, at embryonic day 14.5 just
167 before embryonic lethality (Figure 6). Since it was unlikely to obtain three genotypes of both
168 sexes from the same littermates, the data from mutant neurons were normalized by the ones
169 of *Ambra1*$^{+/+}$ neurons from their littermates.
170 Evoked EPSC (eEPSC) amplitude and total number of synaptic vesicles ready to release,
171 called readily releasable pool (RRP), in *Ambra1*$^{gt/gt}$ neurons were reduced to ~67% in male
172 and ~51% in female, respectively, of control values without change in mEPSC amplitudes and
173 vesicular release probability (P_{vr}) (Figure 6A-D), suggesting that Ambra1 is essential for the
174 activity of excitatory synapse. Interestingly, even in these cultured neurons grown
175 independently and separately, the most prominent alteration depending on sex is that the

176 eEPSC and RRP sizes in female heterozygous neurons, exhibited a decreasing trend, but not
177 in males (Figure 6A-D). Synaptic plasticity upon 10 Hz stimuli was similar between three
178 genotypes (Figure 6E-F). Interestingly, both sexes exhibited approximately 30% of reduction
179 in response to exogeneous application of glutamate in *Ambra1*$^{gt/gt}$, which is different from the
180 change in synaptic responses (Figure 6C-D).
181 We tested whether the reduction of eEPSC amplitude is due to defects in synaptogenesis by
182 the absence of Ambra1. Using immunofluorescent staining of vGluT1 and PSD95 to label
183 glutamatergic pre- and postsynapses in each autaptic neuron, the number of presynaptic and
184 postsynaptic puncta were similar between genotypes, and Mander's overlapping coefficient
185 between vGluT1 and PSD95 signals were comparable between genotypes, indicating that the
186 spatial integrity of pre- and postsynapses were unaffected by Ambra1 (Figure S3). This
187 indicates, even in cultured single neurons, sex-dimorphic changes in synaptic release were
188 detected without alteration in synaptic number, as data in acute brain slices. In order to find
189 out whether the phenotype also occurs in inhibitory input, the similar analysis was performed
190 in autaptic GABAergic neurons cultured from the striatum of female mice at postnatal day 0
191 (Nair et al., 2013). Interestingly, the release machinery and synaptic GABA receptor cluster
192 was not changed in *Ambra1*$^{+/gt}$ neurons (Figure 6G). Our data addressed that *Ambra1*
193 heterozygous mutation produces a pronounced effect restricted to glutamatergic release in
194 females without any environmental factors.
195

196 **Discussion**

197 We characterized the consequence of *Ambra1* heterozygous mutation, known to induce
198 female-specific ASD, by multiple level of analysis including behavioral, biochemical,
199 morphological, and electrophysiological approaches. The remarkable and distinct finding in
200 our study is that the reduced power of γ-oscillations and increased susceptibility to seizure in
201 *Ambra1* heterozygous mice, two proxies of E/I imbalance, occurs exclusively in females
202 (Figure 3). To understand the mechanism underlying this imbalance, we considered the
203 possible contribution of autophagy that may serve as a bridge linking Ambra1 and ASD. This
204 is because autophagy has been known to have a profound relationship with neurodegenerative
205 diseases caused by the accumulation of harmful proteins and damaged organelles and
206 neuronal development diseases such as ASD caused by impairment of neurodevelopmental
207 processes including neurogenesis, neuronal differentiation and synaptic remodeling/function
208 (Gkogkas et al., 2012; Kuijpers et al., 2021; Tang et al., 2014).
209 Our previous study demonstrated a marked brain enlargement in female *Ambra1*$^{+/gt}$ mutant
210 (Mitjans et al., 2017), which is a common feature in human ASD (Courchesne et al., 2011).

211 And Ambra1 protein is also known to be involved in proliferation/apoptosis and its absence
212 induced brain overgrowth in mouse embryos (Maria Fimia et al., 2007). It further strengthened
213 the autophagy hypothesis to support the ASD seen in the *Ambra1*$^{+/gt}$ and led us to speculate
214 that altered populations of different cell types or overgrowth of neuronal morphology, such as
215 dendritic arborization or spine density, may disturb E/I balance and contribute to brain
216 overgrowth.
217 First of all, the current study displays a novel fact that Ambra1 in the brain is only present in
218 neurons, including synapses and it limited the target of Ambra1 function (Figure 1). Moreover,
219 the number of glutamatergic, GABAergic and PV-expressing neurons, dendrite complexity,
220 and spine density is unaltered in *Ambra1*$^{+/gt}$ hippocampal region, indicating no critical effect on
221 the neurogenesis by *Ambra1* heterozygous mutation (Figure 4A-G, Figure 5A-C and Figure
222 S1-2). Crucially, no significant difference is found in autophagic activity between *Ambra1*$^{+/gt}$
223 and *Ambra1*$^{+/+}$ brains (Figure 4H-I), which could be supported by previous data that ~50% of
224 autophagic activity was still observed in *Ambra1*$^{gt/gt}$ embryonic brains (Maria Fimia et al., 2007).
225 Therefore, it can be inferred that the cause of ASD, probably E/I imbalance in *Ambra1*$^{+/gt}$, is far
226 from autophagy activity, which has been known to directly affects axon and synapses (Cheng
227 et al., 2015; Soukup et al., 2016; Soykan et al., 2021; Wang et al., 2015).
228 The oscillatory activity in the neural network is a comprehensive signal of global E/I. To further
229 dissect the cellular substrates underlying the alteration of this E/I signal, we focused on
230 functional synapses rather than morphological ones. The possible cause of E/I imbalance,
231 occurring only in female *Ambra1*$^{+/gt}$ brain slices, is a slight decrease in mEPSC frequency
232 (Figure 5E). This moderate reduction at single cell level, through altering ratio with mIPSC
233 frequency, can be accumulated at the neuronal network level, which contributes as the basis
234 for inducing ASD. That is, even small changes in the number of functional synapses or synaptic
235 activity can cause the E/I imbalance. The finding is highly reminiscent of previous study for
236 *Nlgn4* knockout mice, as a construct-valid and face-valid mouse model of ASD, proposing that
237 the accumulation of subtle local changes in synaptic function yields pronounced perturbation
238 in global network activity (Hammer et al., 2015). We projected the ”little things make great
239 things” into our data. However, it was still not sufficient to explain the mechanism by which
240 ASD occurring in *Ambra1* heterozygous mutation appear only in female.
241 The female-specific behavioral phenotypes had to consider the influence of specific
242 environments *in vivo*, such as unique hormones. To study the neuronal intrinsic change by
243 genetic factors limited to females, eliminate the external effects coming from *in vivo* conditions,
244 and deconvolute the diluted results from E/I input measurement, we specifically analyzed the
245 cultured neurons from very early embryonic day 14.5 just before *Ambra1*$^{gt/gt}$ embryos death
246 (Maria Fimia et al., 2007). As the intrinsic activities of cultured *Ambra1*$^{+/+}$, *Ambra1*$^{+/gt}$, and

247 *Ambra1* $^{gt/gt}$ neurons could be compared simultaneously, it enables us to understand the
248 substantial role of Ambra1 in neurons. As a result, regardless of sex, Ambra1 deficiency had
249 no effect on neuronal development and synapse formation, and decrease selectively the
250 number of functional glutamatergic synapses. Moreover, surprisingly, the cultured *Ambra1*$^{+/gt}$
251 neurons also showed a female-specific decrease in eEPSC size, as the change in mEPSC
252 frequency in *Ambra1*$^{+/gt}$ female brain acute slice (Figure 6A-D). Thus, ASD caused by E/I
253 imbalance in *Ambra1* heterozygous mutation is a neuron-intrinsic property of Ambra1 by sex
254 difference without any environmental factors. And our previous study, the decrease in relative
255 Ambra1 expression level in female *Ambra1*$^{+/gt}$ brain, compared to one in male (Dere et al.,
256 2014), may help to understand the female-specific synaptic phenotype. Thus, we can suggest
257 that the size of EPSCs would be determined according to the expression level of Ambra1
258 protein.
259 In *Ambra1* $^{gt/gt}$ neurons, the comparable mEPSC amplitudes and the eEPSC or mEPSC
260 frequencies reduced in half lead to the novel fact that there are Ambra1-dependent and -
261 independent synapses. In particular, it can be speculated that Ambra1 deficiency makes
262 Ambra1-dependent synapses into silence (Figure 6). And, although Ambra1-dependent
263 synapses maintain silence, the fact that the reduction of glutamate-induced response is less
264 than that of synaptic responses such as eEPSC, mEPSC frequency and RRP size raise two
265 possibilities (Figure 6). Firstly, depletion of functional synaptic receptors that may be induced
266 by Ambra1 deficiency can lead to an increase in the number of extrasynaptic receptors. The
267 other possibility is that the *Ambra1* $^{gt/gt}$ neurons display the complete ablation of synaptic
268 release in Ambra1-dependent synapses. To elucidate the impairment of synaptic release and
269 its relationship to synaptic receptors, we recall our previous work (Sigler et al., 2017). The
270 number of functional synaptic glutamate receptors was reduced by approximately 40% in
271 Munc13-deficient synapses in which synaptic transmission from presynaptic terminal is
272 completely impaired. So, the difference between reduction ratios in synaptic parameters such
273 as the eEPSC size and mEPSC frequency, and glutamate induced responses in *Ambra1*$^{gt/gt}$
274 can be attributed to the complete impairment of glutamate release. In order to support the two
275 hypotheses, it can be inferred that the Ambra1-dependent synapses accounts for about 50%
276 of the total synapses. Considering our data evaluating the expression levels of synaptic
277 receptors and scaffolding proteins (Figure S1), we highly appreciate the latter possibility. We
278 figured out that the most critical factor of E/I imbalance in *Ambra1* heterozygous brain is the
279 contribution of Ambra1 in the activity of glutamatergic synapses, regardless of autophagy. In
280 the end, we discovered that the novel function of Ambra1 in neuronal cells play an important
281 factor in ASD manifestation.

282 We conclude that Ambra1, localized specifically in neuronal cells, intrinsically triggers
283 excitatory synaptic activity, and that its sex-dimorphic expression of protein level modulates
284 the degree of glutamate release depending on sex (Dere et al., 2014). However, the
285 mechanism for the sex-dimorphic expression of Ambra1 protein level is still an important piece
286 to be studied further. This sex-dimorphic reduction of synaptic transmission by *Ambra1*
287 haploinsufficiency might manifest female-specific phenotypes, such as autistic-like behaviors,
288 increased seizure propensity and aberrant gamma oscillations (Dere et al., 2014), which
289 provides us important insight on the neural substrate of E/I balance related with ASD and
290 epilepsy.
291

292 ## Materials and methods

293 *Animals*

294 *Ambra1* mutant mice were described previously(Maria Fimia et al., 2007). Wild-type (WT,
295 *Ambra1*$^{+/+}$) and heterozygous *Ambra1*$^{+/gt}$ (Het) littermates of both sexes with a >99%
296 C57BL/6N genetic background were obtained by interbreeding male *Ambra1*$^{+/gt}$ and female
297 WT C57BL/6N mice and used for all experiments on postnatal animals. For neuronal cultures,
298 *Ambra1*$^{+/+}$, *Ambra1*$^{+/gt}$, and *Ambra1*$^{gt/gt}$ (KO) littermate embryos were obtained by interbreeding
299 male and female *Ambra1*$^{+/gt}$ mice. All experiments were carried out in agreement with the
300 guidelines for the welfare of experimental animals issued by the Federal Government of
301 Germany and Max Planck Society.

302 *Genotyping*

303 Genomic DNA for genotyping was extracted from tail tips of 2-3 week-old offspring or embryos
304 using NucleoSpin Tissue kit (Machery-Nagel GmbH & Co. KG). WT and KO *Ambra1* alleles
305 and Y chromosomes of offspring were detected by polymerase chain reaction (PCR) of
306 genomic DNA. PCR analyses of *Ambra1* KO gene were performed as described
307 previously(Dere et al., 2014) using GoTaq® G2 Flexi DNA polymerase (Promega). For *Ambra1*
308 WT allele, GoTaq® G2 Flexi DNA polymerase (Promega) with forward primer, 5'-AAC TGA
309 ACC TGG GTT CTT TGA A-3' and reverse primer 5'-GAA AAG CTC CCC ATC TTT TCT T-3'
310 were used to generate a 0.5 kb fragment (95°C/5 min, 35 cycles with 95°C/30 s, 57°C/45 s,
311 72°C/105 s, and 72°C/ 10 min). For sex determination of embryos, PCR analyses of Y
312 chromosomes were performed using GoTaq® G2 Flexi DNA polymerase, forward primer 5'-
313 GGT GTG GTC CCG TGG TGA GAG-3', and reverse primer 5'-GAG GCA ACT GCA GGC
314 TGT AAA ATG-3' to generate a 270 bp fragment (94°C/1 min, 33 cycles with 94°C/1 min,

315 63°C/30 s, 72°C/30 s, and 72°C/7 min). PCR products were analyzed on a 1.5% agarose gel
316 in Tris-Acetate-EDTA buffer, which were stained with HDGreen® Plus Safe DNA Dye (Intas).

317 *mRNA expression of Ambra1 from data of Allen Brain Atlas*

318 Data of mRNA expression level in different brain regions were extracted from Allen Mouse
319 Brain Atlas (Figure 1a, http://mouse.brain-map.org/)(Ju et al., 2020; Lein et al., 2007). mRNA
320 expression level in regions of interests (ROIs) of in situ hybridization was calculated by
321 multiplying expression density and intensity.

322 *Histological and Immunohistochemical Analyses*

323 Mice were perfused transcardially with Ringer solution followed by 4% paraformaldehyde (PFA)
324 in 0.1 M phosphate buffer (PBS, pH=7.4). Brains were post-fixed at 4°C in 4% PFA in PBS for
325 2 h for X-galactosidase (X-gal) histochemical staining, or post-fixed overnight, followed by
326 cryo-protection in 30% sucrose solution in PBS and in liquid nitrogen for immunohistochemistry.

327 X-gal histochemical staining was performed with brains of 9 weeks old mice. Coronal brain
328 sections (50 μm) were cut using Leica VT1000S vibrotome (Leica Biosystems) and incubated
329 overnight in the dark at 37°C in X-gal solution containing 5mM $K_3[Fe(CN)_6]$. 5mM $K_4[Fe(CN)_6]$,
330 2mM $MgCl_2$ and 1.2 mg/mL 5-bromo-2-chloro-3 indoyl-b-D-galactopyranoside (X-gal) in PBS,
331 rinsed three times in PBS, and mounted with Aqua-Poly/mount (Polyscience). Digital images
332 were obtained using an Axiophot microscope (Carls Zeiss Microscopy GmbH).

333 *Ambra1* WT and Het female mouse brain were cut into coronal sections (30 μm) with Leica
334 CM1950 instrument (Leica Biosystems). Sections were blocked with 10% normal horse serum
335 (NHS) and 0.2% Triton-X-100 in PBS for 1 h at room temperature (RT). PBS with 5% NHS and
336 0.2% Triton-X-100 was also used for the primary and secondary antibody dilution. Incubation
337 of the primary antibodies was carried out at 4°C for 1-3 nights, followed by incubation of
338 secondary antibodies (1:500) for 2 h and DAPI (1:10,000, D9542, Sigma-Aldrich) in PBS for 5
339 min at RT. Washing was performed between every step and sections were mounted using
340 Aqua-Poly/mount. The following antibodies were used for immuohistochemistry: mouse anti-
341 β-gal (Z3781, Promega), chicken anti-NeuN (266006, Synaptic Systems), rabbit anti-IBA1
342 (019-19741, Wako), rabbit anti-Olig2 (AB9610, Chemicon), rabbit anti-GFAP (G5601,
343 Promega), guinea pig anti-Ctip 2 (325005, Synaptic Systems), mouse anti-GAD67 (MAB5406,
344 Chemicon), rabbit anti-PV (PV27, Swant), Alexa-Fluor 488 donkey anti-mouse IgG (A21202,
345 Invitrogen), Alexa-Fluor 488 donkey anti-chicken IgG (703-546-155, Jackson
346 ImmunoResearch), Alexa-Fluor 488 goat anti-chicken IgG (A-11039, Thermo Fisher Scientific),
347 Alexa-Fluor 555 goat anti-guinea pig IgG (A-21435, Thermo Fisher Scientific), Alexa-Fluor 555

348 goat anti-mouse IgG (A-21424, Thermo Fisher Scientific), Alexa-Fluor 594 goat anti-mouse
349 IgG (115-585-003, Jackson ImmunoResearch), Alexa-Fluor 594 donkey anti-rabbit IgG (A-
350 21207, Invitrogen) and Alexa-Fluor 633 goat anti-rabbit IgG (A-21071, Thermo Fisher
351 Scientific). Leica TCS SP5 confocal microscope (Leica Biosystems) was used to scan
352 anatomically matched sections using 0.5 µm z-step and a 20x objective lens. For counting cell
353 numbers, the dorsal part of hippocampus (Bregma -1.34 to -2.54 mm posterior) was used
354 bilaterally in each animal (12-14 hippocampi per 1-2 animal). Image stacks were further
355 processed by Image J and quantification of CTIP2+, GAD67+ and PV+ were done using Imaris
356 7.5.1 and manually. Cell density was obtained by dividing the number of each cell type by the
357 total volume of hippocampal region in mm^3.

358 *Protein Extraction and Measurement*

359 Cortices of 6-weeks old mice and hippocampi of 4-weeks old mice were dissected in cold 0.32
360 M sucrose solution with protease inhibitors (0.1 µM Aprotinin, 50 µM Leupeptin, 0.2 mM PMSF)
361 and homogenized using glass-teflon homogenizer (900 rpm, 10 strokes). Cortical homognates
362 of male WT and female WT and Het mice at 6 weeks of age were used for purification of
363 synaptic membrane proteins (Fig. 1f). All centrifugations were performed with Beckman TL-
364 100 Ultracentrifuge (Beckman Coulter) at 4°C. Cortical homogenates were layered on a
365 discontinuous gradient of 0.85 M, 1.0 M, and 1.2 M sucrose solutions. After centrifugation at
366 82,500 g for 2 h, the supernatant above 0.85 M sucrose layer and the pellet were kept as
367 soluble fraction (S) and mitochondria-enriched fraction (P2D), respectively. The interface
368 fractions between 0.32 M and 0.85 M sucrose, between 0.85 M and 1.0 M sucrose, and
369 between 1.0 M and1.2 M were collected as myelin-enriched fraction (P2A), ER-Golgi-enriched
370 Fraction (P2B), and synaptosome fraction (P2C), respectively. The P2C fraction was diluted
371 with 0.32 M sucrose solution with protease inhibitors and centrifuged at 100,000 g for 20 min.
372 After centrifugation, the resulting pellet was resuspended in 2.5 mL of 6 mM Tris-Cl, pH 8 and
373 incubated on ice for 45 min for osmotic shock. After centrifugation at 32,800 g for 20 min, the
374 supernatants were collected as synaptic cytoplasm and crude synaptic vesicle (SC/CSV)
375 fractions, and the pellets were resuspended as crude synaptic membrane (CSM) fraction with
376 3 mL of 0.32 M sucrose solution with protease inhibitors. CSM fractions were applied to a
377 discontinuous gradient of 0.85 M, 1.0 M, and 1.2 M sucrose solutions and centrifuged at 82,500
378 g for 2 h. The interface fraction between 1.0 M and 1.2 M sucrose was harvested as pure
379 synaptic membrane fraction (SM) and diluted in 0.32 M Sucrose solution with protease
380 inhibitors, followed by centrifugation at 100,000 g for 20 min. The resulting pellet was re-
381 suspended in 500 µL of 6 mM Tris-Cl pH 8.0. Purified fractions were stored at -80°C. Protein

382 concentrations in various samples were measured using Bradford method (Bio-Rad) according
383 to the manufacturer's instructions.

384 *Western Blotting*

385 SDS-PAGE and protein transfer to nitrocellulose membranes were performed according to
386 standard procedures.(Laemmli, 1970; Towbin et al., 1979) After transfer, the membranes were
387 washed with ultra-pure water and incubated with Memcode Reversible Protein Stain Kit
388 (Thermo Fisher Scientific) according to the manufacturers' protocol. Membranes were washed
389 and incubated in blocking buffer (5% milk powder in Tris-based saline with 0.05 % Tween-20,
390 TBST) for 1 h at RT. followed by incubation with primary antibodies diluted at 1:1000 in
391 blocking buffer for 3 h at RT. Membranes were then incubated with primary antibodies (1:1000)
392 and secondary antibodies (1:5000) with washing three times with TBST for 15 min each
393 between. Protein signals were detected with Odyssey Infrared Imaging System (LI-COR
394 Biosciences GmbH) and quantified using the Image-Studio Software (Odyssey System; LI-
395 COR Biosciences GmbH) with normalization to total protein assessed by Memcode staining.
396 The following antibodies were used for Western blotting: mouse anti-PSD95 (ab2723, Abcam),
397 mouse anti-Gephyrin (147111, Synaptic Systems), rabbit anti-GluR1 (PC246, Calbiochem),
398 rabbit anti-GluR2 (182103, Synaptic Systems), mouse anti-NMDAR1 (114011, Synaptic
399 Systems), rabbit anti-GuR6/7 (04-921, Mllipore), rabbit anti-$GABA_A$Rα1 (Ab5592, Chemicon
400 GmbH), rabbit anti-$GABA_A$Rγ2 (Ab82970, Abcam), rabbit anti-vGluT1 (135302, Synaptic
401 Systems), mouse anti-ß-Tubulin (T4026, Sigma-Aldrich), IRDye680-anti-mouse IgG (926-
402 68070, LI-COR Biosciences GmbH), IRDye800-anti-rabbit IgG (926-32211, LI-COR
403 Biosciences GmbH).

404 *Pentylenetetrazol (PTZ)-Induced Seizures*

405 Seizure activity was induced in awake 12-13 weeks-old Ambra1 WT and Het mice of both
406 sexes by a single intraperitoneal (i.p.) injection of 50 mg of Pentylenetetrazol (PTZ; P6500,
407 Sigma-Aldrich) per 1 kg of body weight. After injection, mice were observed closely for 30 min
408 in a small clear home cage. Four phases of behavioral response to PTZ injection were defined
409 as follows: (1) Hypoactivity; decrease in mobility until the animal arrests in a crouched posture.
410 (2) Partial clonus (PC), clonic seizure activity in face, head, and forelimbs. (3) Generalized
411 clonus (GC); sudden loss of upright posture, whole body clonus including all four limbs and tail,
412 rearing and autonomic signs. (4) Tonic-clonic (TC) (maximal) seizure; generalized seizure with
413 tonic hind-limb extension followed by death. The latency to GC and the seizure score, which
414 is calculated from the latencies to PC, GC, and TC in seconds by equation [Seizure score =
415 1000 / (0.2 * PC latency + 0.3 * GC latency + 0.5 * TC latency)] were used as measures(Wojcik
416 et al., 2013).

417 *Electrophysiological recordings*

418 Four weeks old WT and *Ambra1* Het mice were anesthetized with Isofluorane and decapitated.
419 During the entire procedure, carbogen gas (95% oxygen and 5% carbon dioxide) keeps
420 applied in solutions. The whole brain was immediately transferred to cold slicing solution (230
421 mM Sucrose, 26 mM $NaHCO_3$, 1 m KH_2PO_4, 2 mM KCl, 2 mM $MgCl_2x6H_2O$, 10 mM Glucose,
422 0.5 mM $CaCl_2$). To get hippocampal slices for evoke field excitatory postsynaptic potentials
423 (fEPSP) recording, hippocampi were isolated carefully and cut transversally at 300 µm
424 thickness using a McILWAIN tissue chopper (Molecular Devices, LLC). For acute brain slices,
425 sagittal sections at 5° angle tilted to the midline with 300 µm thickness were obtained inside
426 the same slicing solution at 4°C using Leica VT1200S vibrotome (Leica Biosystems). Slices
427 were immediately transferred to a chamber filled with artificial cerebrospinal fluid (ACSF; 120
428 mM NaCl, 26 mM $NaHCO_3$, 1 m KH_2PO_4, 2 mM KCl, 2 mM $MgCl_2x6H_2O$, 10 mM Glucose, 2
429 mM $CaCl_2$) at 37ºC for 1h 40min for hippocampal slices and at 37°C for 20 min for acute brain
430 slices. After recovery, slices were kept at RT.

431 For fEPSP measurement, the hippocampal slices were placed in interface recording chamber
432 (Harvard Apparatus) with continuous flow of carbogen-supplied ACSF at 30ºC. An electric
433 stimulation was applied with 100 µs duration time by concentric metal bipolar electrode (FHC)
434 on the *Stratum radiatum* of Schaffer collaterals. Recording electrode (2-3 MΩ) was pulled from
435 thin-walled borosilicate glass capillaries, filled with ACSF, and positioned on the *Stratum*
436 *radiatum* of CA1 area.

437 For kainite-induced gamma oscillation recording, acute brain slices were placed on interface
438 recording chamber with application of ACSF at 33°C. Recording electrode (2-3 MΩ), filled with
439 ACSF, was placed in the CA3 pyramidal layer of hippocampus. For each slice, baseline field
440 potentials were recorded for 30 min in ACSF, followed by recording of oscillatory field potentials
441 in gamma-range induced by 100 nM kainic acid (BN0281, BIOTREND Chemikalien GmbH) in
442 ACSF for 30 min. After this recording phase, the electrode was slightly re-positioned to acquire
443 the maximum power of gamma oscillation for another 10 min. Recordings were acquired by
444 Multiclamp 700B amplifier and Digidata 1440A (Molecular Devices, LLC.) and data were
445 analyzed using AxographX (Axograph), as previously described(Ripamonti et al., 2017).

446 For whole-cell recordings, the somata of hippocampal CA1 pyramidal neurons in acute brain
447 slice were whole-cell voltage clamped at -70 mV by recording electrode (2.5-3.5 MΩ)
448 containing internal solution with 100 mM KCl, 50 mM K-gluconate, 10 mM HEPES, 4 mM ATP-
449 Mg, 0.3 mM GTP-Na, 0.1 mM EGTA, 0.4% biocytin, pH 7.4, 300 mOsm. The external solution
450 was carbogen-saturated ACSF. Miniature excitatory and inhibitory post-synaptic currents
451 (mEPSCs/mIPSCs) were recorded in the presence of 1 µM TTX, mixed with 10 µM bicuculine

452 methiodide for measuring mEPSCs or with 10 µM NBQX for measuring mIPSCs with washing
453 with 1 µM TTX for 15 mins between. An EPC-10 amplifier with Patchmaster v2X80 software
454 was used for data acquisition (HEKA/Harvard Bioscience). Subsequently, slices were fixed
455 using 4% PFA in PBS for two hours at RT and washed by PBS.

456 *Immunohistochemistry of Biocytin-filled Neurons*

457 After being washed in PBS, blocked and permeabilized for 1h with blocking solution (5% NGS
458 and 0.5% Triton X-100 in PBS), fixed brain slices obtained from patching were stained with
459 Alexa-Fluor-555-labeled streptavidin (1:1000; S32355, Thermo Fisher Scientific.) and DAPI
460 (1:10,000) in blocking solution. After washing, the slices were mounted on glass slides and
461 covered with cover slips in Aqua-Poly/Mount. CA1 pyramidal neurons in hippocampus were
462 scanned using a Leica SP5 confocal microscope with 100 x/1.44 NA oil objective at 0.126 µm
463 z-intervals. The basal and apical part of pyramidal neurons 3D Gaussian-filtered ($\sigma_{x,y}$ 0.7, σ_z
464 0.7,), using custom-written macros to handle the large data sets. Only cells with a pyramidal
465 shape and a location in CA1 were used for further analysis.

466 *In Utero Electroporation and Immunohistochemistry for Sholl Analysis*

467 E14.5 mouse embryos from WT mothers bred with Het males were subjected to IUE (permit
468 number 33.19-42502-04-13/1052), as previously described(dal Maschio et al., 2012; Hsia et
469 al., 2014). DNA solution with pFUGW (0.1 mg/mL) and pCX::myrVENUS (0.1 mg/mL) for the
470 myrVenus construct(Lois et al., 2002; Rhee et al., 2006) were used to sparsely label CA1
471 pyramidal neurons in hippocampus.

472 *In utero* electroporated mice were perfused, and brains were post-fixed and cryo-protected
473 (15%-30% sucrose in PBS) at P28. Coronal brain sections (230 µm thickness) at -1.06 mm to
474 -2.46 mm from Bregma were collected using a Leica VT 1000S vibrotome. For
475 immunofluorescence staining, PFA was quenched by 1 mg/mL $NaBH_4$ in PBS for 5 min
476 followed byh thorough washing in PBS. Brain sections were incubated in blocking solution (5%
477 normal goat serum (NGS) and 0.5 % Triton-X-100 in PBS) for 1 h at RT followed by incubation
478 in 0.2% Tween-20 and 10 µg/mL heparin in PBS for 1.5 h to improve the penetration of
479 antibody in thick brain sections. The blocking solution was used for diluting primary and
480 secondary antibodies (1:1000 dilution). The sections were incubated with polyclonal rabbit anti-
481 GFP antibody (598, MBL) for 4 days at 4°C and with Alexa-Fluor (AF) 488 goat anti-rabbit IgG
482 (R37116, Thermo Fisher Scientific) overnight at RT followed by DAPI staining (1:10,000) and
483 mounted on slides. Images of CA1 pyramidal neurons in hippocampus were acquired with 1.02

484 μm z-steps by Leica SP2 confocal microscope (Leica Biosystems) and oil-immersion 20x
485 objective.

486 *Analysis of Neuron Morphology using NeuronStudio*

487 For segmentation of entire dendritic trees and subsequent mushroom spine analysis, we used
488 NeuronStudio (CNIC, Mount Sinai School of Medicine, New York, NY, USA)(Rodriguez et al.,
489 2008). After reconstructing the dendritic trees, 3D Sholl analysis from this program was
490 performed to acquire the accumulative dendritic length in every 10 μm step from the center of
491 soma.(Sholl, 1953) Mushroom spines were automatically detected along the reconstructed
492 dendritic tress using the NeuronStudio segmentation algorithm by keeping the suggested
493 parameters(Rodriguez et al., 2008; Sigler et al., 2017) (Head diameter of mushroom spines:
494 0.35 μm) and the numbers of mushroom spines were counted every 10 μm from the center of
495 soma.

496 *Autaptic Neuron Culture and Electrophysiology*

497 Autaptic cultures of cortical glutamatergic neurons from hippocampi from E14.5 embronic
498 brains or striatum of P0 postnatal brains were prepared according to a previously published
499 protocol(Jockusch et al., 2007) with slight modifications. 3,000 to 3,500 cells were plated on
500 35 mm^2 coverslips with astrocyte islands in Neurobasal-A Medium with supplements.

501 Autaptic neurons were analyzed electrophysiologically as described previously(Kawabe et al.,
502 2010) at day in vitro (DIV) 10-16. Autaptic neruons were whole-cell voltage clamped at -70 mV
503 with a MultiClamp700B amplifier (Axon Instruments, Molecular Devices) under the control of
504 the Clampex program 10.1 (Molecular Devices). The internal solution for recording autaptic
505 neurons consisted of 136 mM KCl, 17.8 mM HEPES, 1 mM EGTA, 4.6 mM $MgCl_2$, 4 mM
506 NaATP, 0.3 mM Na_2GTP, 15 mM creatine phosphate, and 5 units/mL phospho-creatine kinase
507 (315-320 mosmol/L), pH7.4. Extracellular solution contained 140 mM NaCl, 2.4 mM KCl, 10
508 mM HEPES, 10mM glucose, 4 mM $CaCl_2$, and 4 mM $MgCl_2$ (320 mosmol/L), pH 7.3. All
509 chemicals were purchased from Sigma-Aldrich (Sigma-Aldrich) unless mentioned otherwise.

510 Evoked post synaptic currents (PSCs) were measured by depolarization of neurons from -70
511 to 0 mV for 2 ms. Readily releasable vesicle pool size (RRP) was recorded by measuring PSC
512 in response to application of 0.5 M hypertonic sucrose in extracellular solution. P_{vr} was
513 calculated by dividing the charge transfer during an action potential-evoked response by the
514 charge transfer measured during a response to hypertonic solution. Additionally, EPSC
515 amplitudes were measured after application of 50 stimuli at 10 Hz to assess short-term
516 depression. Glutamate-induced response was measured by focal application of 100 μM

517 glutamic acid (Sigma) in order to study the cell surface expression of glutamate receptor.
518 mEPSCs were recorded in the presence of 300 mM TTX (Tocris). Given that three genotypes
519 of identical sex are difficult to obtain in the same litters, the data were normalized to WT mean
520 values obtained in several sets of experiments.

521 *Immunofluorescent staining and analysis of pre- and post-synaptic puncta in autaptic neurons*

522 At DIV 18-23 from two independent cell preparation, autaptic cultured neurons were fixed in a
523 solution containing 4% PFA/4% sucrose in PBS, pH7.4, for 20 min. After washing with PBS for
524 3 times, cells were incubated in blocking solution containing 0.3% Triton-X-100, 10% NGS and
525 0.1% fish skin gelatin (Sigma) in PBS for 20 min. Neurons were incubated with primary
526 antibodies against vGluT1 (1:1000, rabbit polyclonal, 135303, Synaptic Systems), PSD95
527 (1:200, mouse monoclonal, ab2723, Abcam), and MAP2 (1:500, chicken polyclonal, NB300-
528 213, Novus biologicals) diluted in blocking solution for overnight at 4°C. After repetitive
529 washing with PBS, neurons were incubated with secondary antibodies diluted in blocking
530 solution, including Alexa-Fluor 488 goat anti-chicken IgG (1:1000, A-21441, Invitrogen), Alexa-
531 Fluor 555 goat anti-rabbit IgG (1:1000, A-32732, Invitrogen) and Alexa-Fluor 633 goat anti-
532 mouse IgG (1:1000, A-21052, Invitrogen) for 2 hrs at RT, followed by another rounds of
533 washing. After DAPI staining, coverslips were mounted on slides.

534 Single autaptic neurons were imaged by Leica SP2 confocal microscope using 40x objective
535 (resolution: 1024 x 1024 pixels) with 1 μm z-step and analyzed using Image J software, as
536 referenced from previous publication(Ripamonti et al., 2017). Briefly, for the quantification of
537 pre- and post-syanptic puncta, the fluorescent signals of vGlut and PSD95 were thresholded
538 and binarized followed by being watersheded. The number of their puncta was analyzed using
539 'Analyze particle' option. For the colocalization of pre- and post-synaptic marker, the
540 Manders' overlap coefficient was calculated by Intensity Correlation Analysis plugin.

541 *Statistical Analysis*

542 All data were analyzed separately for males and females. Statistical methods are described in
543 figure legends. All statistics were performed with Excel (Microsoft), GraphPad Prism 5 software
544 (GraphPad software) and SPSS 17 (SPSS Inc.). Data are presented as mean±S.E.M., and p-
545 values <0.05 were considered as indicating a significant difference.
546

547 ## Acknowledgment

548 We thank F. Benseler, for valuable advice and excellent technical support. We are grateful to
549 the staffs at the animal facility of the Max Planck Institute for Multidisciplinary Sciences for
550 mouse husbandry.

551 # Additional information

552 ## Funding

Funder	Grant reference number	Author
European Commission	H2020, Comorbidity and Synapse Biology in Clinically Overlapping Psychiatric Disorders, Project ID 667301	Jeongseop Rhee, Nils Brose
Max Planck Society	open access funding	Jeongseop Rhee, Nils Brose, Hannelore Ehrenreich
DFG	CNMPB	Hannelore Ehrenreich
EXTRABRAIN	EU-FP7	Hannelore Ehrenreich
Niedersachsen-Research Network on Neuroinfectiology (N-RENNT)	open access funding	Hannelore Ehrenreich
European Union's Seventh Framework Program (FP7/2007–2013), the EFPIA companies and Autism Speaks	EU-AIMS	Hannelore Ehrenreich

553 The funders had no role in study design, data collection and interpretation, or the decision to
554 submit the work for publication.

555

556 ## Author contributions

557 Conceptualization: JSR and AJ; Methodology: JSR, AJ, BA, HJR, AS, HE, IH, MS, HK;
558 Investigation: JSR, AJ, BA, HJR, HE, IH, MS, HK; Writing (Original draft): JS and AJ; Writing
559 (review & editing): JS, AJ and NB; Funding acquisition: JSR, NB and HE; Resources: JSR, NB
560 and HE; Supervision: JSR
561 Nils Brose (NB) is under competing interests for being a reviewing editor of this journal. Other
562 authors declare that there is no competing of interest.

563

564 ## Ethics

All experiments were carried out in agreement with the guidelines for the welfare of experimental animals issued by the Federal Government of Germany and Max Planck Society.

Data availability

Most of data generated or analyzed during this study are included in the manuscript and supporting files.

572 **Figure**

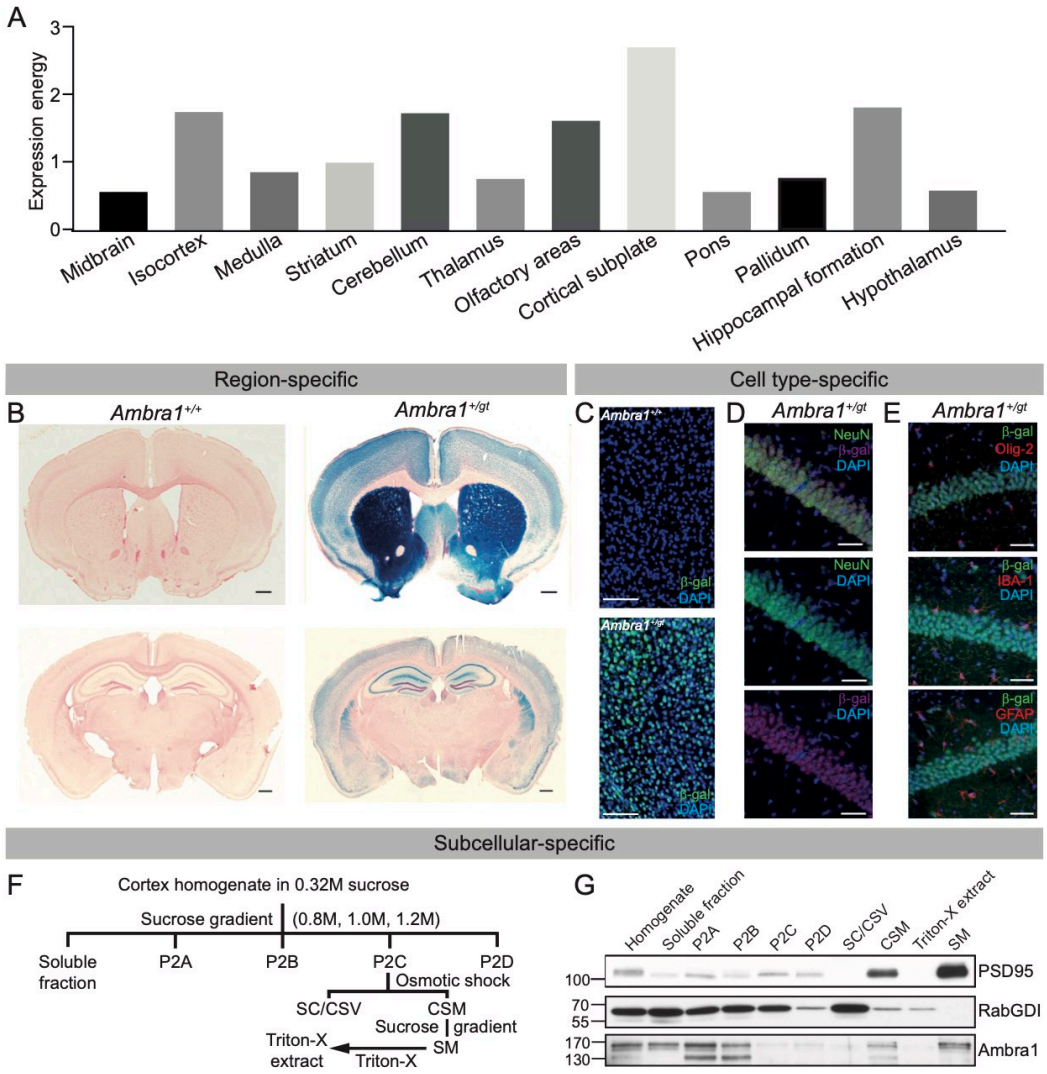

573

574 **Figure 1: Region-, cell type- and subcellular specific location of Ambra1 protein in the**
575 **brain**

576 **A** Expression level of Ambra1 mRNA in different brain regions of a mouse (n=1). **B** X-
577 galactosidase staining in coronal brain section of *Ambra1*$^{+/+}$ and *Ambra1*$^{+/gt}$ mice. Scale bar,
578 100 µm. **C** Immunofluorescence staining of β-galactosidase (β-gal). **D, E** Co-staining of β-gal
579 with different cellular markers, including neuronal marker, NeuN (**D**) or glial markers, Olig-2,
580 IBA-1 and GFAP (**E**) in hippocampal CA1 pyramidal region of *Ambra1*$^{+/gt}$ mouse. Scale bar, 40
581 µm. **F** Schematic representation of the subcellular fractionation step. P2A, Myelin-enriched
582 fraction; P2B, ER/Golgi-enriched fraction; P2C, Synaptosome fraction; P2D, Nucleus- and
583 mitochondria-enriched fraction; SC, Synaptic cytoplasm; CSV, Crude synaptic vesicles; CSM,
584 Crude synaptic membrane; SM, Pure Synaptic Membrane Fractions. **G** Western blots of
585 PSD95, RabGDI and Ambra1 proteins in subcellular fractions of *Ambra1*$^{+/+}$ mouse cerebral
586 cortex. PSD95 and RabGDI were used for verification of purification of SM fraction.

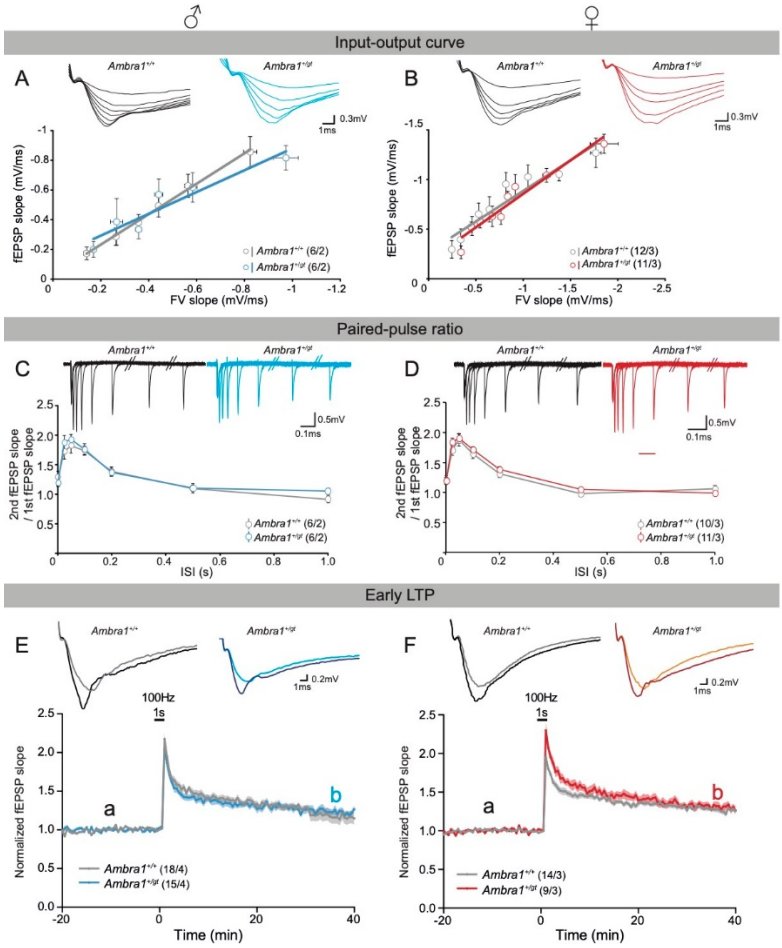

Figure 2: Activity-dependent synaptic transmission and short- and long-term synaptic plasticity of hippocampal CA1

Left panel contains data from male mice, while right panel represents data from female mice. Field excitatory postsynaptic potential (fEPSP) slope was recorded in the *Striatum Radiatum* of CA1 upon Schaffer-Collateral stimulation in acute hippocampal slice. **A, B** Input-output curve from *Ambra1*$^{+/+}$ (black) and *Ambra1*$^{+/gt}$ (color) mice in both sexes. fEPSP slopes were measured after increasing the stimulus intensity and plotted along their fiber volley (FV) slopes. **C, D** Paired-pulse ratio curve from two genotypes in both sexes. Ratios of 2nd and 1st fEPSP slope (Paired-pulse ratio) after two stimuli within different time intervals (Interstimulus interval, ISI) were plotted along their respective intervals. Representative traces were shown within graphs. **E, F** Early-phase long-term potentiation (E-LTP) from two genotypes in both sexes. fEPSP slopes after stimuli every 30 second were normalized to baseline and plotted along time. After 20 minutes of baseline, a high frequency stimulation (100 Hz for 1 sec) was given to induce potentiation. Representative traces are shown within graphs (light color: baseline, dark color: potentiation). N numbers are written next to the legend within the graphs and shown as slice number/animal number. Mean ± S.E.M. are presented in line and area and statistical difference was defined by p-value between genotypes from Repeated-Measures of ANOVA.

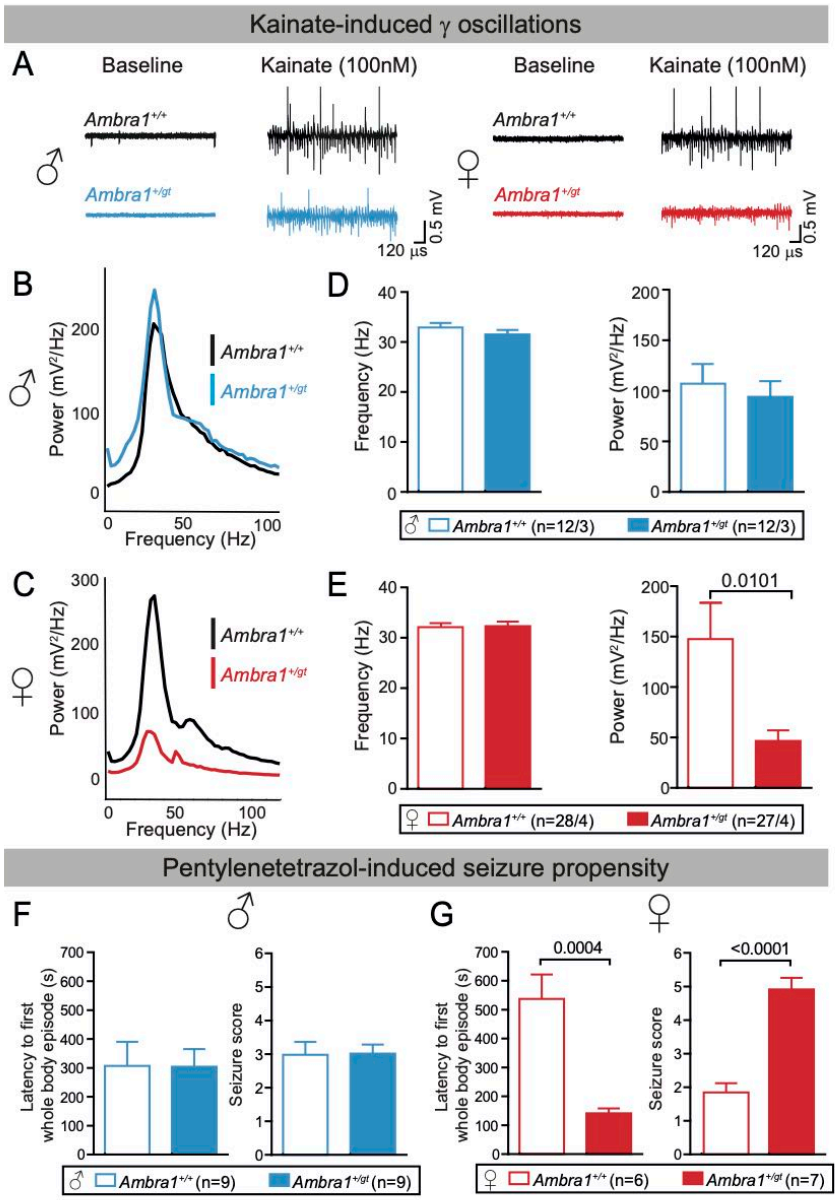

Figure 3: Perturbed γ-power and seizure propensity only in *Ambra1*$^{+/gt}$ females but not in males

A Representative traces of **γ-**oscillations before and during being induced by 100 nM kainate in hippocampal CA3 pyramidal layer of acute brain slices in *Ambra1*$^{+/+}$ and *Ambra1*$^{+/gt}$ male and female mice. **B, C** Representative power spectrums of gamma oscillations are shown. **D, E** Quantifications of the frequency of maximum power and average power within gamma range (25-45 Hz) at 4 weeks old. **F, G** Latency to first whole-body episode and seizure score were measured during observation after injection of pentylenetetrazol (50mg/kg) in 12-13 weeks old mice. The bar graphs are presented as mean ± S.E.M and slice number/animal number or animal numbers of each group are noted next to the legends. Statistical analysis between *Ambra1*$^{+/+}$ and *Ambra1*$^{+/gt}$ was performed by two-tailed unpaired t-test with significance level $p < 0.05$.

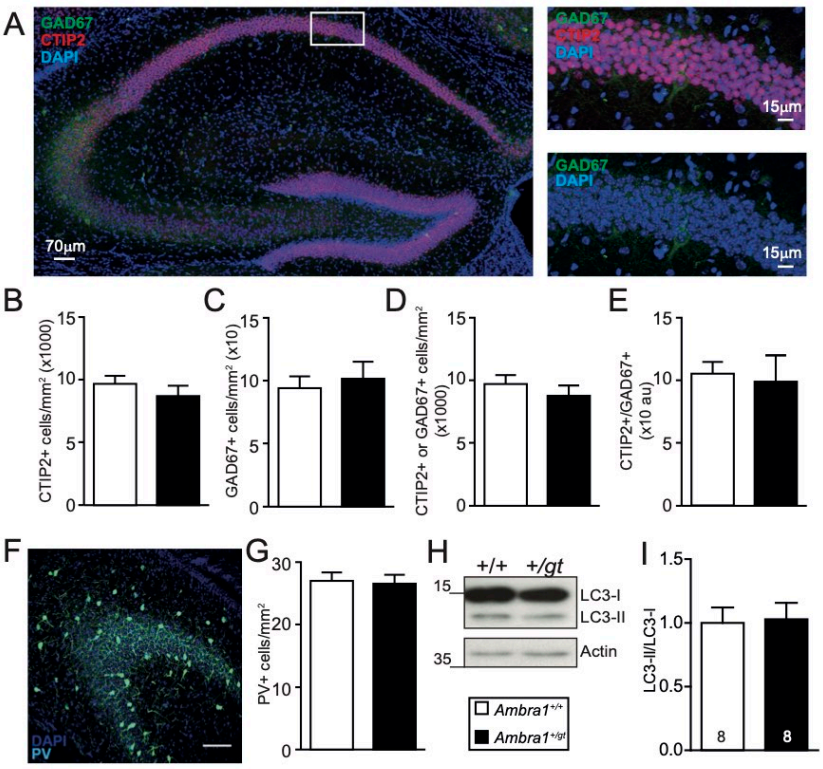

Figure 4: Comparable neuronal numbers and autophagic activity in the brains of *Ambra1*$^{+/+}$ and *Ambra1*$^{+/gt}$ mice

A Example images of hippocampal CA1 region immunostained with anti-CTIP2 and anti-GAD67 antibodies. **B-E** The quantifications of the density of CTIP2+ (**B**), GAD67+ (**C**), sum of CTIP2+ and GAD67+ neurons (**D**) and ratio of CTIP2+ and GAD67+ neurons (**E**) in *Ambra1*$^{+/+}$ and *Ambra1*$^{+/gt}$ mouse hippocampus. **F** Example images of hippocampal CA3 region immunostained with an anti-PV antibody. 4 weeks old wild type mouse was used. **G** The quantifications of PV+ neurons in *Ambra1*$^{+/+}$ and *Ambra1*$^{+/gt}$ mouse hippocampus. 13-15 sections in 1-2 animals were used for analysis per group. **H** Sample picture of LC3 Western Blot between cortical homogenates of both genotypes (n=8 for each group) in female mice. The data was normalized to the average value of wild-type group. **I** Comparison of LC3-II and LC3-I intensities between two genotypes. The bar graphs represent mean ± S.E.M and statistical analysis was performed by two-tailed unpaired t-test with significance level $p < 0.05$.

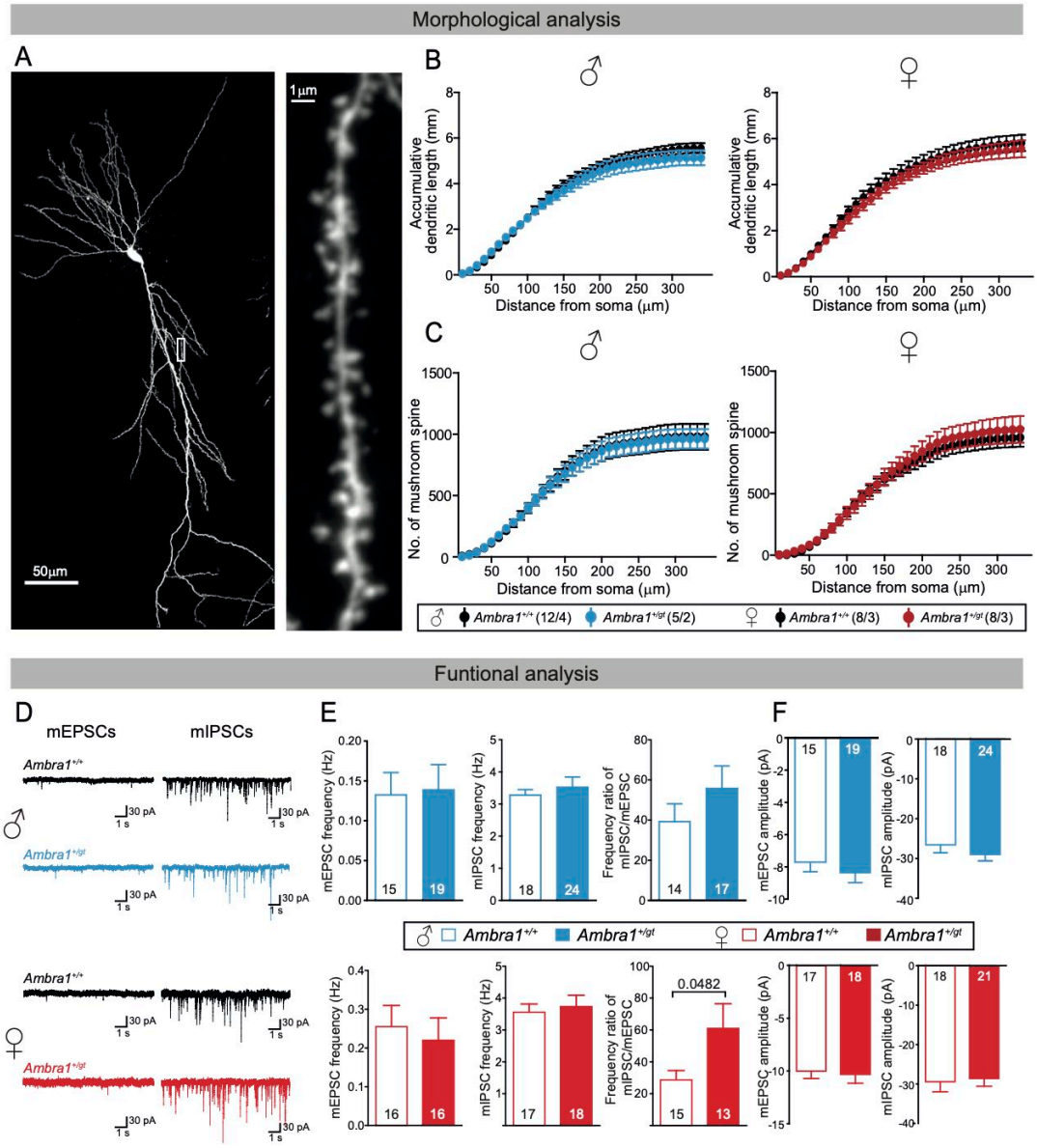

Figure 5: Imbalance of excitatory and inhibitory inputs upon *Ambra1* heterozygous mutation in female-specific manner

A Example images of CA1 pyramidal neuron. **B, C** Accumulative dendritic length (**B**) and number of mushroom-shaped spines (**C**) were plotted along the distance from soma Numbers written in brackets next to the legends represent neuron numbers/animal numbers. **D** Representative traces of mEPSC with 10μM bicuculine and mIPSC with 10μM NBQX from both genotypes. **E, F** The frequencies of mEPSC and mIPSC, frequency ratio of mIPSC/mEPSC (**E**), and amplitudes of mEPSC and mIPSC (**F**) in two genotypes of male (upper) and female (lower) mice. Numbers written within bars represent neuron numbers acquired from 4-5 animals per group. All experiments were performed at 4 weeks old. The spots and bars represent mean ± S.E.M and statistical analysis was performed by two-way ANOVA (**B, C**) and two-tailed unpaired t-test (**E, F**) with significance level $p < 0.05$.

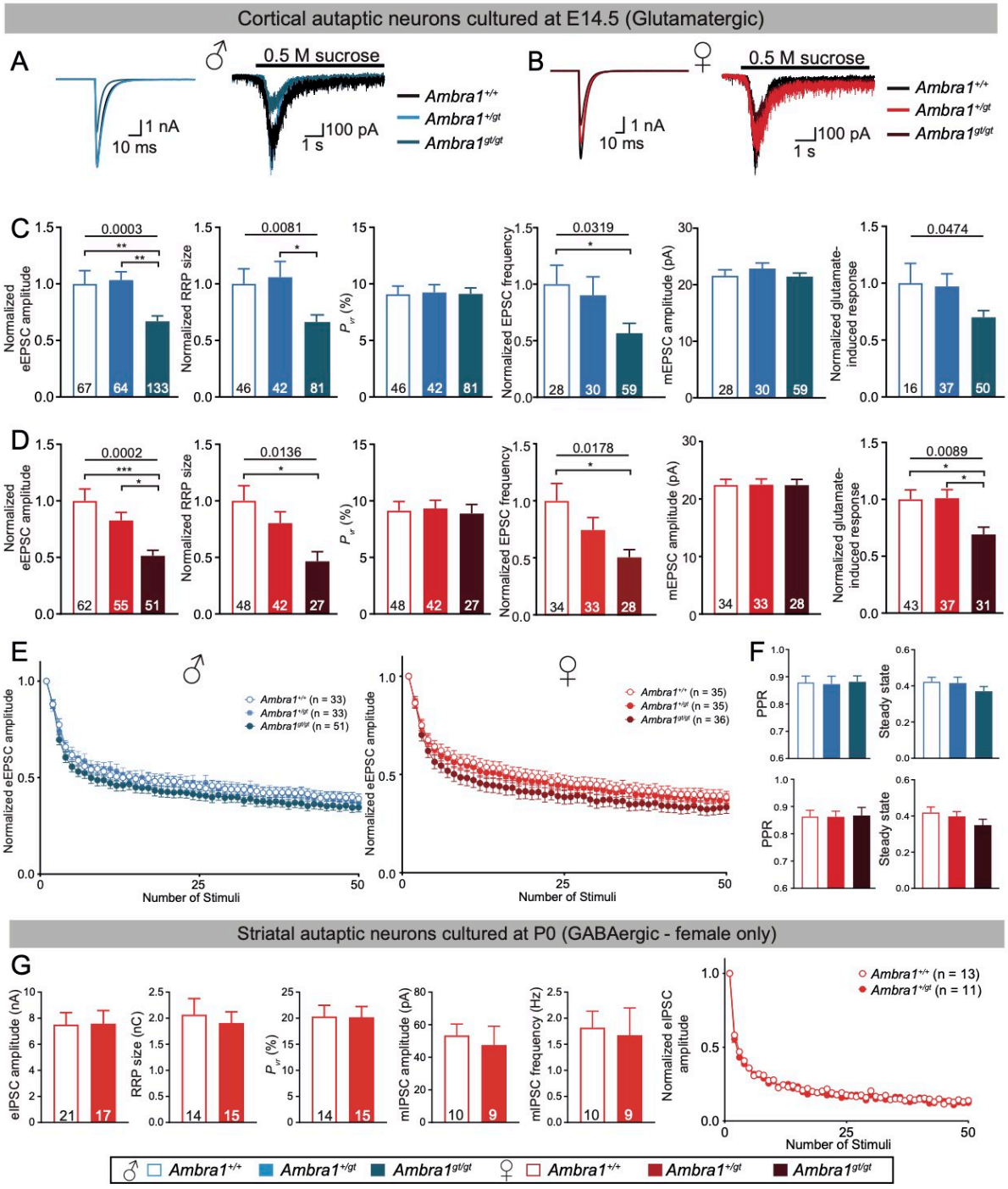

Figure 6: Aberrant synaptic transmission in the absence of *Ambra1* gene, regardless of sex

A, B Sample traces of eEPSC and 0.5 M sucrose-induced response from glutamatergic autaptic neurons from E14.5 hippocampal-like embryonic brain of *Ambra1*$^{+/+}$, *Ambra1*$^{+/gt}$ and *Ambra1*$^{gt/gt}$ in males (**A**) and females (**B**). **C, D** The bar graphs of normalized eEPSC amplitude, normalized RRP size, P_{vr}, normalized mEPSC frequency, mEPSC amplitude and 100µM glutamate-induced response between three genotypes in males (**C**) and females (**D**), separately. **E** Short-term synaptic depression was monitored after application of 50 stimuli at

655 10 Hz. **F** Comparison of normalized eEPSC amplitude acquired from 2nd stimuli (Paired pulse
656 ratio (PPR), left) and averaged during the steady state (36-40th stimuli, right) from 10 Hz
657 stimulation experiment (**E**). **G** The bar graphs of eIPSC amplitude, RRP size, P_{vr} and
658 amplitudes and frequency of mIPSC and a dot graph of short-term synaptic depression by 50
659 stimuli at 10 Hz in GABAergic autaptic neurons from P0 striatum of *Ambra1*$^{+/+}$ and *Ambra1*$^{+/gt}$
660 females. Neuron numbers of each group are written within the bar or next to the legends from
661 2-4 independent experiments and the bars and dots in graphs are presented as mean ± S.E.M.
662 Statistical analysis of bar graphs from three groups (**C, D, and F**) was performed by one-way
663 ANOVA followed by Bonferroni or Tukey post-hoc test showing significance as asterisk (*,
664 p≤0.05; **, p≤0.01; ***, p≤0.001) and from two groups (**G**) by two-tailed unpaired t-test with
665 significance below 0.05. Short-term synaptic depression (**E, G**) was analyzed by Repeated
666 Measures of ANOVA.
667

668 ## References

669 Association AP. 2013. Diagnostic and Statistical Manual of Mental Disorders, Diagnostic and
670 Statistical Manual of Mental Disorders. American Psychiatric Association.
671 doi:10.1176/appi.books.9780890425596.x00DiagnosticClassification
672 Baron-Cohen S, Lombardo M V., Auyeung B, Ashwin E, Chakrabarti B, Knickmeyer R. 2011.
673 Why Are Autism Spectrum Conditions More Prevalent in Males? *PLoS Biol* **9**:e1001081.
674 doi:10.1371/journal.pbio.1001081
675 Bermejo MK, Milenkovic M, Salahpour A, Ramsey AJ. 2014. Preparation of Synaptic Plasma
676 Membrane and Postsynaptic Density Proteins Using a Discontinuous Sucrose Gradient.
677 *J Vis Exp* 51896. doi:10.3791/51896
678 Bolton PF, Carcani-Rathwell I, Hutton J, Goode S, Howlin P, Rutter M. 2011. Epilepsy in autism:
679 features and correlates. *Br J Psychiatry* **198**:289–294. doi:10.1192/bjp.bp.109.076877
680 Bourgeron T. 2015. From the genetic architecture to synaptic plasticity in autism spectrum
681 disorder. *Nat Rev Neurosci* **16**:551–563. doi:10.1038/nrn3992
682 Chakrabarti S, Fombonne E. 2001. Pervasive Developmental Disorders in Preschool Children.
683 *JAMA* **285**:3093–3099. doi:10.1001/JAMA.285.24.3093
684 Cheng XT, Zhou B, Lin MY, Cai Q, Sheng ZH. 2015. Axonal autophagosomes recruit dynein
685 for retrograde transport through fusion with late endosomes. *J Cell Biol* **209**:377–386.
686 doi:10.1083/JCB.201412046/VIDEO-1
687 Courchesne E, Mouton PR, Calhoun ME, Semendeferi K, Ahrens-Barbeau C, Hallet MJ,
688 Barnes CC, Pierce K. 2011. Neuron Number and Size in Prefrontal Cortex of Children
689 With Autism. *JAMA* **306**:2001. doi:10.1001/jama.2011.1638
690 dal Maschio M, Ghezzi D, Bony G, Alabastri A, Deidda G, Brondi M, Sato SS, Zaccaria RP, Di
691 Fabrizio E, Ratto GM, Cancedda L. 2012. High-performance and site-directed in utero
692 electroporation by a triple-electrode probe. *Nat Commun* **3**:960.
693 doi:10.1038/ncomms1961
694 Delorme R, Ey E, Toro R, Leboyer M, Gillberg C, Bourgeron T. 2013. Progress toward
695 treatments for synaptic defects in autism. *Nat Med* **19**:685–694. doi:10.1038/nm.3193
696 Dere E, Dahm L, Lu D, Hammerschmidt K, Ju A, Tantra M, KÃ¤stner A, Chowdhury K,
697 Ehrenreich H, Kästner A, Chowdhury K, Ehrenreich H. 2014. Heterozygous Ambra1
698 Deficiency in Mice: A Genetic Trait with Autism-Like Behavior Restricted to the Female
699 Gender. *Front Behav Neurosci* **8**:181. doi:10.3389/fnbeh.2014.00181
700 Ebert DH, Greenberg ME. 2013. Activity-dependent neuronal signalling and autism spectrum
701 disorder. *Nature* **493**:327–337. doi:10.1038/nature11860

702 Elsabbagh M, Divan G, Koh Y-J, Kim YS, Kauchali S, Marcín C, Montiel-Nava C, Patel V,
703 Paula CS, Wang C, Yasamy MT, Fombonne E. 2012. Global Prevalence of Autism and
704 Other Pervasive Developmental Disorders. *Autism Res* **5**:160–179. doi:10.1002/aur.239
705 Epilepsy and autism spectrum disorders may have a shared aetiology. 2016. . *Nat Rev Neurol*
706 **12**:430–430. doi:10.1038/nrneurol.2016.100
707 Gkogkas CG, Khoutorsky A, Ran I, Rampakakis E, Nevarko T, Weatherill DB, Vasuta C, Yee
708 S, Truitt M, Dallaire P, Major F, Lasko P, Ruggero D, Nader K, Lacaille J-CC, Sonenberg
709 N. 2012. Autism-related deficits via dysregulated eIF4E-dependent translational control.
710 *Nature* **493**:371–377. doi:10.1038/nature11628
711 Hammer M, Krueger-Burg D, Tuffy LP, Cooper BH, Taschenberger H, Goswami SP,
712 Ehrenreich H, Jonas P, Varoqueaux F, Rhee J-S, Brose N. 2015. Perturbed Hippocampal
713 Synaptic Inhibition and γ-Oscillations in a Neuroligin-4 Knockout Mouse Model of Autism.
714 *Cell Rep* **13**:516–523. doi:10.1016/j.celrep.2015.09.011
715 Heiniger H. J. H-J, Dorey. 1989. Handbook on Genetically Standardized JAX Mice, 4th editio.
716 ed. The Jackson Laboratory, Bar Harbor.
717 Hsia H-E, Kumar R, Luca R, Takeda M, Courchet J, Nakashima J, Wu S, Goebbels S, An W,
718 Eickholt BJ, Polleux F, Rotin D, Wu H, Rossner MJ, Bagni C, Rhee J-S, Brose N, Kawabe
719 H. 2014. Ubiquitin E3 ligase Nedd4-1 acts as a downstream target of PI3K/PTEN-
720 mTORC1 signaling to promote neurite growth. *Proc Natl Acad Sci U S A* **111**:13205–10.
721 doi:10.1073/pnas.1400737111
722 Huang Y, Jiang H, Zheng Q, Fok AHK, Li X, Lau CG, Lai CSW. 2021. Environmental
723 enrichment or selective activation of parvalbumin-expressing interneurons ameliorates
724 synaptic and behavioral deficits in animal models with schizophrenia-like behaviors during
725 adolescence. *Mol Psychiatry* **26**:2533–2552. doi:10.1038/s41380-020-01005-w
726 Jockusch WJ, Speidel D, Sigler A, Sørensen JB, Varoqueaux F, Rhee J-S, Brose N. 2007.
727 CAPS-1 and CAPS-2 are essential synaptic vesicle priming proteins. *Cell* **131**:796–808.
728 doi:10.1016/j.cell.2007.11.002
729 Ju A, Fernandez-Arroyo B, Wu Y, Jacky D, Beyeler A. 2020. Expression of serotonin 1A and
730 2A receptors in molecular- And projection-defined neurons of the mouse insular cortex.
731 *Mol Brain* **13**:1–13.
732 Kawabe H, Neeb A, Dimova K, Young SM, Takeda M, Katsurabayashi S, Mitkovski M,
733 Malakhova OA, Zhang D-E, Umikawa M, Kariya K, Goebbels S, Nave K-A, Rosenmund
734 C, Jahn O, Rhee J, Brose N. 2010. Regulation of Rap2A by the ubiquitin ligase Nedd4-1
735 controls neurite development. *Neuron* **65**:358–72. doi:10.1016/j.neuron.2010.01.007
736 Kuijpers M, Kochlamazashvili G, Stumpf A, Puchkov D, Swaminathan A, Lucht MT, Krause E,
737 Maritzen T, Schmitz D, Haucke V. 2021. Neuronal Autophagy Regulates Presynaptic

738 Neurotransmission by Controlling the Axonal Endoplasmic Reticulum. *Neuron* **109**:299-
739 313.e9. doi:10.1016/J.NEURON.2020.10.005
740 Laemmli UK. 1970. Cleavage of Structural Proteins during the Assembly of the Head of
741 Bacteriophage T4. *Nature* **227**:680–685.
742 Lee BH, Smith T, Paciorkowski AR. 2015. Autism spectrum disorder and epilepsy: Disorders
743 with a shared biology. *Epilepsy Behav* **47**:191–201. doi:10.1016/J.YEBEH.2015.03.017
744 Lein ES, Hawrylycz MJ, Ao N, Ayres M, Bensinger A, Bernard A, Boe AF, Boguski MS,
745 Brockway KS, Byrnes EJ, Chen Lin, Chen Li, Chen T-M, Chi Chin M, Chong J, Crook BE,
746 Czaplinska A, Dang CN, Datta S, Dee NR, Desaki AL, Desta T, Diep E, Dolbeare TA,
747 Donelan MJ, Dong H-W, Dougherty JG, Duncan BJ, Ebbert AJ, Eichele G, Estin LK, Faber
748 C, Facer BA, Fields R, Fischer SR, Fliss TP, Frensley C, Gates SN, Glattfelder KJ,
749 Halverson KR, Hart MR, Hohmann JG, Howell MP, Jeung DP, Johnson RA, Karr PT,
750 Kawal R, Kidney JM, Knapik RH, Kuan CL, Lake JH, Laramee AR, Larsen KD, Lau C,
751 Lemon TA, Liang AJ, Liu Y, Luong LT, Michaels J, Morgan JJ, Morgan RJ, Mortrud MT,
752 Mosqueda NF, Ng LL, Ng R, Orta GJ, Overly CC, Pak TH, Parry SE, Pathak SD, Pearson
753 OC, Puchalski RB, Riley ZL, Rockett HR, Rowland SA, Royall JJ, Ruiz MJ, Sarno NR,
754 Schaffnit K, Shapovalova N V., Sivisay T, Slaughterbeck CR, Smith SC, Smith KA, Smith
755 BI, Sodt AJ, Stewart NN, Stumpf K-R, Sunkin SM, Sutram M, Tam A, Teemer CD, Thaller
756 C, Thompson CL, Varnam LR, Visel A, Whitlock RM, Wohnoutka PE, Wolkey CK, Wong
757 VY, Wood M, Yaylaoglu MB, Young RC, Youngstrom BL, Feng Yuan X, Zhang B,
758 Zwingman TA, Jones AR. 2007. Genome-wide atlas of gene expression in the adult
759 mouse brain. *Nature* **445**:168–176. doi:10.1038/nature05453
760 Li K, Nakajima M, Ibañez-Tallon I, Heintz N. 2016. A Cortical Circuit for Sexually Dimorphic
761 Oxytocin-Dependent Anxiety Behaviors. *Cell* **167**:60-72.e11.
762 doi:10.1016/j.cell.2016.08.067
763 Lois C, Hong EJ, Pease S, Brown EJ, Baltimore D. 2002. Germline transmission and tissue-
764 specific expression of transgenes delivered by lentiviral vectors. *Science* **295**:868–72.
765 doi:10.1126/science.1067081
766 Malishkevich A, Amram N, Hacohen-Kleiman G, Magen I, Giladi E, Gozes I. 2015. Activity-
767 dependent neuroprotective protein (ADNP) exhibits striking sexual dichotomy impacting
768 on autistic and Alzheimer's pathologies. *Transl Psychiatry* **5**:e501.
769 doi:10.1038/tp.2014.138
770 Maria Fimia G, Stoykova A, Romagnoli A, Giunta L, Di Bartolomeo S, Nardacci R, Corazzari
771 M, Fuoco C, Ucar A, Schwartz P, Gruss P, Piacentini M, Chowdhury K, Cecconi F. 2007.
772 Ambra1 regulates autophagy and development of the nervous system. *Nature* **447**:1121–
773 1125. doi:10.1038/nature05925

774 Martinerie J, Adam C, Quyen ML Van, Baulac M, Clemenceau S, Renault B, Varela FJ. 1998.
775 Epileptic seizures can be anticipated by non-linear analysis. *Nat Med* **4**:1173–1176.
776 doi:10.1038/2667
777 Mathalon DH, Sohal VS, G B, BJ R, RT C, J N, CA B, P T, Y H. 2015. Neural Oscillations and
778 Synchrony in Brain Dysfunction and Neuropsychiatric Disorders. *JAMA Psychiatry*
779 **72**:840–844. doi:10.1001/jamapsychiatry.2015.0483
780 Mitjans M, Begemann M, Ju A, Dere E, Wüstefeld L, Hofer S, Hassouna I, Balkenhol J, Oliveira
781 B, van der Auwera S, Tammer R, Hammerschmidt K, Völzke H, Homuth G, Cecconi F,
782 Chowdhury K, Grabe H, Frahm J, Boretius S, Dandekar T, Ehrenreich H. 2017. Sexual
783 dimorphism of AMBRA1-related autistic features in human and mouse. *Transl Psychiatry*
784 **7**:e1247–e1247. doi:10.1038/tp.2017.213
785 Nair R, Lauks J, Jung SY, Cooke NE, de Wit H, Brose N, Kilimann MW, Verhage M, Rhee JS.
786 2013. Neurobeachin regulates neurotransmitter receptor trafficking to synapses. *J Cell*
787 *Biol* **200**:61–80. doi:10.1083/JCB.201207113
788 Nelson SB, Valakh V. 2015. Excitatory/Inhibitory Balance and Circuit Homeostasis in Autism
789 Spectrum Disorders. *Neuron* **87**:684–698. doi:10.1016/j.neuron.2015.07.033
790 Nobili A, Krashia P, Cordella A, La Barbera L, Dell'Acqua MC, Caruso A, Pignataro A, Marino
791 R, Sciarra F, Biamonte F, Scattoni ML, Ammassari-Teule M, Cecconi F, Berretta N, Keller
792 F, Mercuri NB, D'Amelio M. 2018. Ambra1 Shapes Hippocampal Inhibition/Excitation
793 Balance: Role in Neurodevelopmental Disorders. *Mol Neurobiol* **55**:7921–7940.
794 doi:10.1007/s12035-018-0911-5
795 Rhee JM, Pirity MK, Lackan CS, Long JZ, Kondoh G, Takeda J, Hadjantonakis A-K. 2006. In
796 vivo imaging and differential localization of lipid-modified GFP-variant fusions in
797 embryonic stem cells and mice. *genesis* **44**:202–218. doi:10.1002/dvg.20203
798 Ripamonti S, Ambrozkiewicz MC, Guzzi F, Gravati M, Biella G, Bormuth I, Hammer M, Tuffy
799 LP, Sigler A, Kawabe H, Nishimori K, Toselli M, Brose N, Parenti M, Rhee J. 2017.
800 Transient oxytocin signaling primes the development and function of excitatory
801 hippocampal neurons. *Elife* **6**. doi:10.7554/eLife.22466
802 Rodriguez A, Ehlenberger DB, Dickstein DL, Hof PR, Wearne SL. 2008. Automated Three-
803 Dimensional Detection and Shape Classification of Dendritic Spines from Fluorescence
804 Microscopy Images. *PLoS One* **3**:e1997. doi:10.1371/journal.pone.0001997
805 Rossi PG, Parmeggiani A, Bach V, Santucci M, Visconti P. 1995. EEG features and epilepsy
806 in patients with autism. *Brain Dev* **17**:169–174. doi:10.1016/0387-7604(95)00019-8
807 Sholl DA. 1953. Dendritic organization in the neurons of the visual and motor cortices of the
808 cat. *J Anat* **87**:387-406.1.

809 Sigler A, Oh WC, Imig C, Altas B, Kawabe H, Cooper BH, Kwon H-BB, Rhee J-SS, Brose N.
810 2017. Formation and Maintenance of Functional Spines in the Absence of Presynaptic
811 Glutamate Release. *Neuron* **94**:304-311.e4. doi:10.1016/j.neuron.2017.03.029
812 Soukup SF, Kuenen S, Vanhauwaert R, Manetsberger J, Hernández-Díaz S, Swerts J,
813 Schoovaerts N, Vilain S, Gounko N V., Vints K, Geens A, De Strooper B, Verstreken P.
814 2016. A LRRK2-Dependent EndophilinA Phosphoswitch Is Critical for Macroautophagy
815 at Presynaptic Terminals. *Neuron* **92**:829–844. doi:10.1016/J.NEURON.2016.09.037
816 Soykan T, Haucke V, Kuijpers M. 2021. Mechanism of synaptic protein turnover and its
817 regulation by neuronal activity. *Curr Opin Neurobiol* **69**:76–83.
818 doi:10.1016/J.CONB.2021.02.006
819 Spence SJ, Schneider MT. 2009. The Role of Epilepsy and Epileptiform EEGs in Autism
820 Spectrum Disorders. *Pediatr Res* **65**:599–606. doi:10.1203/PDR.0b013e31819e7168
821 Sun Y, Ren G, Ren J, Wang Q. 2021. High-frequency oscillations detected by
822 electroencephalography as biomarkers to evaluate treatment outcome, mirror
823 pathological severity and predict susceptibility to epilepsy. *Acta Epileptol* **3**:29.
824 doi:10.1186/s42494-021-00063-z
825 Tang G, Gudsnuk K, Kuo S-HH, Cotrina MLL, Rosoklija G, Sosunov A, Sonders MSS, Kanter
826 E, Castagna C, Yamamoto A, Yue Z, Arancio O, Peterson BSS, Champagne F, Dwork
827 AJJ, Goldman J, Sulzer D. 2014. Loss of mTOR-Dependent Macroautophagy Causes
828 Autistic-like Synaptic Pruning Deficits. *Neuron* **83**:1131–1143.
829 doi:10.1016/j.neuron.2014.07.040
830 Towbin H, Staehelin T, Gordon J. 1979. Electrophoretic transfer of proteins from
831 polyacrylamide gels to nitrocellulose sheets: procedure and some applications. *Proc Natl*
832 *Acad Sci U S A* **76**:4350–4354.
833 Vos T, Allen C, Arora M, Barber RM, Bhutta ZA, Brown A, Carter A, Casey DC, Charlson FJ,
834 Chen AZ, Coggeshall M, Cornaby L, Dandona L, Dicker DJ, Dilegge T, Erskine HE, Ferrari
835 AJ, Fitzmaurice C, Fleming T, Forouzanfar MH, Fullman N, Gething PW, Goldberg EM,
836 Graetz N, Haagsma JA, Hay SI, Johnson CO, Kassebaum NJ, Kawashima T, Kemmer L,
837 Khalil IA, Kinfu Y, Kyu HH, Leung J, Liang X, Lim SS, Lopez AD, Lozano R, Marczak L,
838 Mensah GA, Mokdad AH, Naghavi M, Nguyen G, Nsoesie E, Olsen H, Pigott DM, Pinho
839 C, Rankin Z, Reinig N, Salomon JA, Sandar L, Smith A, Stanaway J, Steiner C, Teeple
840 S, Thomas BA, Troeger C, Wagner JA, Wang H, Wanga V, Whiteford HA, Zoeckler L,
841 Abajobir AA, Abate KH, Abbafati C, Abbas KM, Abd-Allah F, Abraham B, Abubakar I,
842 Abu-Raddad LJ, Abu-Rmeileh NME, Ackerman IN, Adebiyi AO, Ademi Z, Adou AK, Afanvi
843 KA, Agardh EE, Agarwal A, Kiadaliri AA, Ahmadieh H, Ajala ON, Akinyemi RO, Akseer N,
844 Al-Aly Z, Alam K, Alam NKM, Aldhahri SF, Alegretti MA, Alemu ZA, Alexander LT, Alhabib

S, Ali R, Alkerwi A, Alla F, Allebeck P, Al-Raddadi R, Alsharif U, Altirkawi KA, Alvis-Guzman N, Amare AT, Amberbir A, Amini H, Ammar W, Amrock SM, Andersen HH, Anderson GM, Anderson BO, Antonio CAT, Aregay AF, Ärnlöv J, Artaman A, Asayesh H, Assadi R, Atique S, Avokpaho EFGA, Awasthi A, Quintanilla BPA, Azzopardi P, Bacha U, Badawi A, Balakrishnan K, Banerjee A, Barac A, Barker-Collo SL, Bärnighausen T, Barregard L, Barrero LH, Basu A, Bazargan-Hejazi S, Beghi E, Bell B, Bell ML, Bennett DA, Bensenor IM, Benzian H, Berhane A, Bernabé E, Betsu BD, Beyene AS, Bhala N, Bhatt S, Biadgilign S, Bienhoff K, Bikbov B, Biryukov S, Bisanzio D, Bjertness E, Blore J, Borschmann R, Boufous S, Brainin M, Brazinova A, Breitborde NJK, Brown J, Buchbinder R, Buckle GC, Butt ZA, Calabria B, Campos-Nonato IR, Campuzano JC, Carabin H, Cárdenas R, Carpenter DO, Carrero JJ, Castañeda-Orjuela CA, Rivas JC, Catalá-López F, Chang J-C, Chiang PP-C, Chibueze CE, Chisumpa VH, Choi J-YJ, Chowdhury R, Christensen H, Christopher DJ, Ciobanu LG, Cirillo M, Coates MM, Colquhoun SM, Cooper C, Cortinovis M, Crump JA, Damtew SA, Dandona R, Daoud F, Dargan PI, das Neves J, Davey G, Davis AC, Leo D De, Degenhardt L, Gobbo LC Del, Dellavalle RP, Deribe K, Deribew A, Derrett S, Jarlais DC Des, Dharmaratne SD, Dhillon PK, Diaz-Torné C, Ding EL, Driscoll TR, Duan L, Dubey M, Duncan BB, Ebrahimi H, Ellenbogen RG, Elyazar I, Endres M, Endries AY, Ermakov SP, Eshrati B, Estep K, Farid TA, Farinha CS e S, Faro A, Farvid MS, Farzadfar F, Feigin VL, Felson DT, Fereshtehnejad S-M, Fernandes JG, Fernandes JC, Fischer F, Fitchett JRA, Foreman K, Fowkes FGR, Fox J, Franklin RC, Friedman J, Frostad J, Fürst T, Futran ND, Gabbe B, Ganguly P, Gankpé FG, Gebre T, Gebrehiwot TT, Gebremedhin AT, Geleijnse JM, Gessner BD, Gibney KB, Ginawi IAM, Giref AZ, Giroud M, Gishu MD, Giussani G, Glaser E, Godwin WW, Gomez-Dantes H, Gona P, Goodridge A, Gopalani SV, Gotay CC, Goto A, Gouda HN, Grainger R, Greaves F, Guillemin F, Guo Y, Gupta Rahul, Gupta Rajeev, Gupta V, Gutiérrez RA, Haile D, Hailu AD, Hailu GB, Halasa YA, Hamadeh RR, Hamidi S, Hammami M, Hancock J, Handal AJ, Hankey GJ, Hao Y, Harb HL, Harikrishnan S, Haro JM, Havmoeller R, Hay RJ, Heredia-Pi IB, Heydarpour P, Hoek HW, Horino M, Horita N, Hosgood HD, Hoy DG, Htet AS, Huang H, Huang JJ, Huynh C, Iannarone M, Iburg KM, Innos K, Inoue M, Iyer VJ, Jacobsen KH, Jahanmehr N, Jakovljevic MB, Javanbakht M, Jayaraman SP, Jayatilleke AU, Jee SH, Jeemon P, Jensen PN, Jiang Y, Jibat T, Jimenez-Corona A, Jin Y, Jonas JB, Kabir Z, Kalkonde Y, Kamal R, Kan H, Karch A, Karema CK, Karimkhani C, Kasaeian A, Kaul A, Kawakami N, Keiyoro PN, Kemp AH, Keren A, Kesavachandran CN, Khader YS, Khan AR, Khan EA, Khang Y-H, Khera S, Khoja TAM, Khubchandani J, Kieling C, Kim P, Kim C, Kim D, Kim YJ, Kissoon N, Knibbs LD, Knudsen AK, Kokubo Y, Kolte D, Kopec JA, Kosen S, Kotsakis GA, Koul PA, Koyanagi A, Kravchenko M, Defo

BK, Bicer BK, Kudom AA, Kuipers EJ, Kumar GA, Kutz M, Kwan GF, Lal A, Lalloo R, Lallukka T, Lam H, Lam JO, Langan SM, Larsson A, Lavados PM, Leasher JL, Leigh J, Leung R, Levi M, Li Yichong, Li Yongmei, Liang J, Liu S, Liu Y, Lloyd BK, Lo WD, Logroscino G, Looker KJ, Lotufo PA, Lunevicius R, Lyons RA, Mackay MT, Magdy M, Razek A El, Mahdavi M, Majdan M, Majeed A, Malekzadeh R, Marcenes W, Margolis DJ, Martinez-Raga J, Masiye F, Massano J, McGarvey ST, McGrath JJ, McKee M, McMahon BJ, Meaney PA, Mehari A, Mejia-Rodriguez F, Mekonnen AB, Melaku YA, Memiah P, Memish ZA, Mendoza W, Meretoja A, Meretoja TJ, Mhimbira FA, Millear A, Miller TR, Mills EJ, Mirarefin M, Mitchell PB, Mock CN, Mohammadi A, Mohammed S, Monasta L, Hernandez JCM, Montico M, Mooney MD, Moradi-Lakeh M, Morawska L, Mueller UO, Mullany E, Mumford JE, Murdoch ME, Nachega JB, Nagel G, Naheed A, Naldi L, Nangia V, Newton JN, Ng M, Ngalesoni FN, Nguyen Q Le, Nisar MI, Pete PMN, Nolla JM, Norheim OF, Norman RE, Norrving B, Nunes BP, Ogbo FA, Oh I-H, Ohkubo T, Olivares PR, Olusanya BO, Olusanya JO, Ortiz A, Osman M, Ota E, PA M, Park E-K, Parsaeian M, de Azeredo Passos VM, Caicedo AJP, Patten SB, Patton GC, Pereira DM, Perez-Padilla R, Perico N, Pesudovs K, Petzold M, Phillips MR, Piel FB, Pillay JD, Pishgar F, Plass D, Platts-Mills JA, Polinder S, Pond CD, Popova S, Poulton RG, Pourmalek F, Prabhakaran D, Prasad NM, Qorbani M, Rabiee RHS, Radfar A, Rafay A, Rahimi K, Rahimi-Movaghar V, Rahman M, Rahman MHU, Rahman SU, Rai RK, Rajsic S, Ram U, Rao P, Refaat AH, Reitsma MB, Remuzzi G, Resnikoff S, Reynolds A, Ribeiro AL, Blancas MJR, Roba HS, Rojas-Rueda D, Ronfani L, Roshandel G, Roth GA, Rothenbacher D, Roy A, Sagar R, Sahathevan R, Sanabria JR, Sanchez-Niño MD, Santos IS, Santos JV, Sarmiento-Suarez R, Sartorius B, Satpathy M, Savic M, Sawhney M, Schaub MP, Schmidt MI, Schneider IJC, Schöttker B, Schwebel DC, Scott JG, Seedat S, Sepanlou SG, Servan-Mori EE, Shackelford KA, Shaheen A, Shaikh MA, Sharma R, Sharma U, Shen J, Shepard DS, Sheth KN, Shibuya K, Shin M-J, Shiri R, Shiue I, Shrime MG, Sigfusdottir ID, Silva DAS, Silveira DGA, Singh A, Singh JA, Singh OP, Singh PK, Sivonda A, Skirbekk V, Skogen JC, Sligar A, Sliwa K, Soljak M, Søreide K, Sorensen RJD, Soriano JB, Sposato LA, Sreeramareddy CT, Stathopoulou V, Steel N, Stein DJ, Steiner TJ, Steinke S, Stovner L, Stroumpoulis K, Sunguya BF, Sur P, Swaminathan S, Sykes BL, Szoeke CEI, Tabarés-Seisdedos R, Takala JS, Tandon N, Tanne D, Tavakkoli M, Taye B, Taylor HR, Ao BJ Te, Tedla BA, Terkawi AS, Thomson AJ, Thorne-Lyman AL, Thrift AG, Thurston GD, Tobe-Gai R, Tonelli M, Topor-Madry R, Topouzis F, Tran BX, Truelsen T, Dimbuene ZT, Tsilimbaris M, Tura AK, Tuzcu EM, Tyrovolas S, Ukwaja KN, Undurraga EA, Uneke CJ, Uthman OA, van Gool CH, Varakin YY, Vasankari T, Venketasubramanian N, Verma RK, Violante FS, Vladimirov SK, Vlassov VV, Vollset SE,

917 Wagner GR, Waller SG, Wang L, Watkins DA, Weichenthal S, Weiderpass E, Weintraub
918 RG, Werdecker A, Westerman R, White RA, Williams HC, Wiysonge CS, Wolfe CDA,
919 Won S, Woodbrook R, Wubshet M, Xavier D, Xu G, Yadav AK, Yan LL, Yano Y, Yaseri
920 M, Ye P, Yebyo HG, Yip P, Yonemoto N, Yoon S-J, Younis MZ, Yu C, Zaidi Z, Zaki MES,
921 Zeeb H, Zhou M, Zodpey S, Zuhlke LJ, Murray CJL. 2016. Global, regional, and national
922 incidence, prevalence, and years lived with disability for 310 diseases and injuries, 1990–
923 2015: a systematic analysis for the Global Burden of Disease Study 2015. *Lancet*
924 **388**:1545–1602. doi:10.1016/S0140-6736(16)31678-6
925 Wang T, Martin S, Papadopulos A, Harper CB, Mavlyutov TA, Niranjan D, Glass NR, Cooper-
926 White JJ, Sibarita JB, Choquet D, Davletov B, Meunier FA. 2015. Control of
927 Autophagosome Axonal Retrograde Flux by Presynaptic Activity Unveiled Using
928 Botulinum Neurotoxin Type A. *J Neurosci* **35**:6179–6194.
929 doi:10.1523/JNEUROSCI.3757-14.2015
930 Wojcik SMSM, Tantra M, Stepniak B, Man MK-N, Müller-Ribbe K, Begemann M, Ju A, Papiol
931 S, Ronnenberg A, Gurvich A, Shin Y, Augustin I, Brose N, Ehrenreich H, Man K-NM,
932 Muller-Ribbe K, Begemann M, Ju A, Papiol S, Ronnenberg A, Gurvich A, Shin Y, Augustin
933 I, Brose N, Ehrenreich H. 2013. Genetic markers of a Munc13 protein family member,
934 BAIAP3, are gender specifically associated with anxiety and benzodiazepine abuse in
935 mice and humans. *Mol Med* **19**:135–148. doi:10.2119/molmed.2013.00033
936 Xue M, Atallah B V., Scanziani M. 2014. Equalizing excitation–inhibition ratios across visual
937 cortical neurons. *Nature* **511**:596–600. doi:10.1038/nature13321
938 Zikopoulos B, Barbas H. 2013. Altered neural connectivity in excitatory and inhibitory cortical
939 circuits in autism. *Front Hum Neurosci* **7**:609. doi:10.3389/fnhum.2013.00609
940
941

Supplemental Information

Developmental features in this mouse line

A previous publication has reported alterations in synaptic plasticity, pyramidal neuron spine density and number of parvalbumin-expressing neurons in the hippocampus of adult mice (8 weeks old) restricted to females, whereas we observed no difference in our 4 week-old mice (Nobili et al., 2018). Therefore, we hypothesized that the developmental stage is a pivotal factor to explain the neural substrate underlying and the prepubertal stage is very critical time window in this mouse line. We previously reported very interesting developmental features in seizure propensity, showing opposite transition from protective response to seizure induction in female mutants of 3 weeks old to reduced survival in 13 months old (Mitjans et al., 2017). Here, we added seizure susceptibility at 12 weeks old where this transition already happened, indicating developmental progression of seizure propensity in this mouse line (Mitjans et al., 2017).

Reference

Mitjans M, Begemann M, Ju A, Dere E, Wüstefeld L, Hofer S, Hassouna I, Balkenhol J, Oliveira B, van der Auwera S, Tammer R, Hammerschmidt K, Völzke H, Homuth G, Cecconi F, Chowdhury K, Grabe H, Frahm J, Boretius S, Dandekar T, Ehrenreich H. 2017. Sexual dimorphism of AMBRA1-related autistic features in human and mouse. *Transl Psychiatry* **7**:e1247–e1247. doi:10.1038/tp.2017.213

Nobili A, Krashia P, Cordella A, La Barbera L, Dell'Acqua MC, Caruso A, Pignataro A, Marino R, Sciarra F, Biamonte F, Scattoni ML, Ammassari-Teule M, Cecconi F, Berretta N, Keller F, Mercuri NB, D'Amelio M. 2018. Ambra1 Shapes Hippocampal Inhibition/Excitation Balance: Role in Neurodevelopmental Disorders. *Mol Neurobiol* **55**:7921–7940. doi:10.1007/s12035-018-0911-5

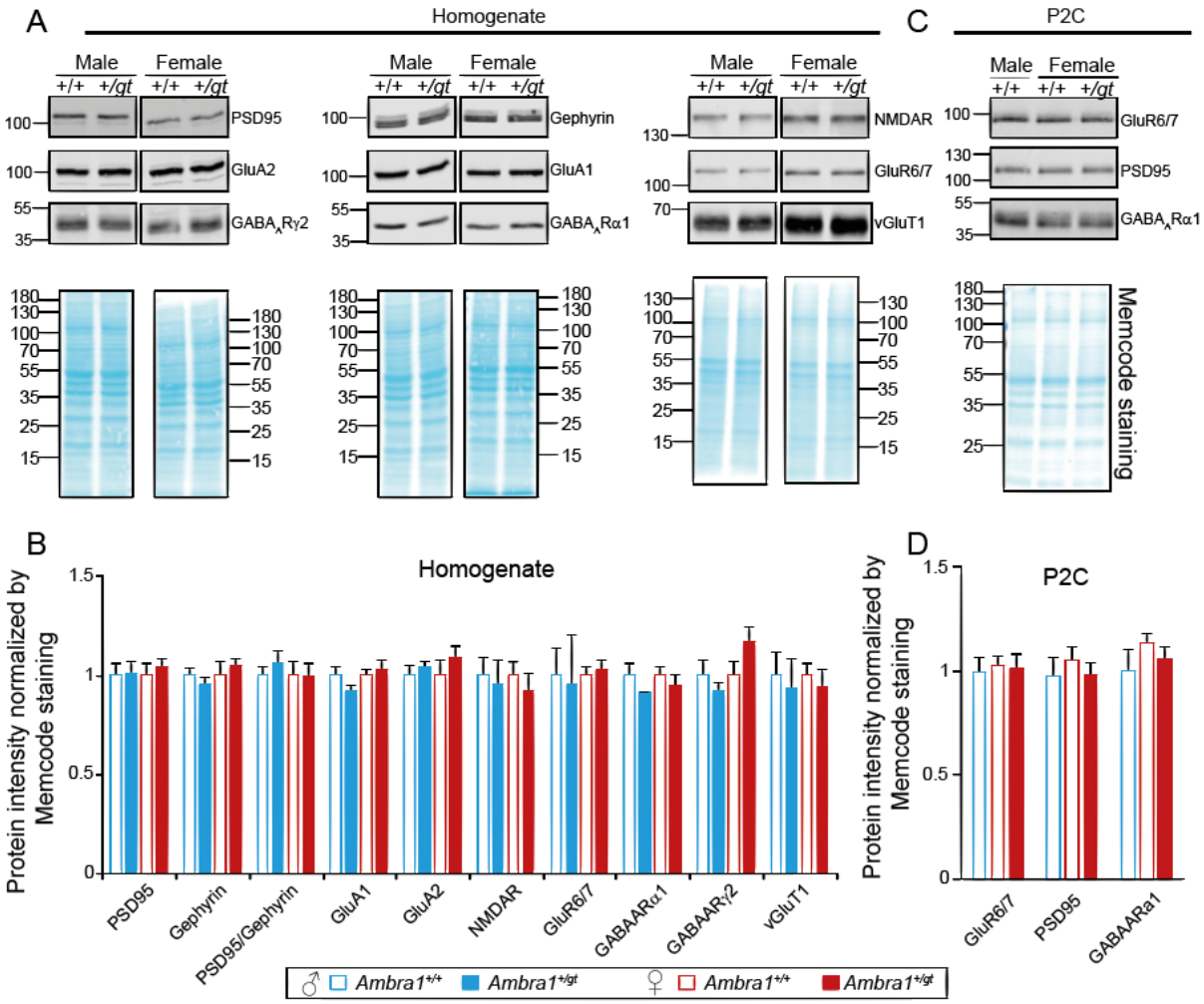

Supplementary Figure S1: Quantification of synaptic proteins in homogenate and synaptosomes

Sample pictures of synaptic proteins (**A, C**) and corresponding Memcode staining and their quantification (**B, D**) were obtained from hippocampal homogenates of *Ambra1*$^{+/+}$ (+/+) and *Ambra1*$^{+/gt}$ (*+/gt*) in 4 week-old males and females (**A, B**) and cortical P2C of 6 week-old male +/+ and female +/+ and *+/gt* (**C, D**). The intensity of synaptic proteins was normalized by corresponding MemCode staining as the amount of total proteins and normalized by the average value of male wild-type group. 3-7 mice were used per each group. The bar graphs represent mean ± S.E.M and statistical analysis between two genotypes were carried out by two-tailed unpaired t-test with significance level $p < 0.05$.

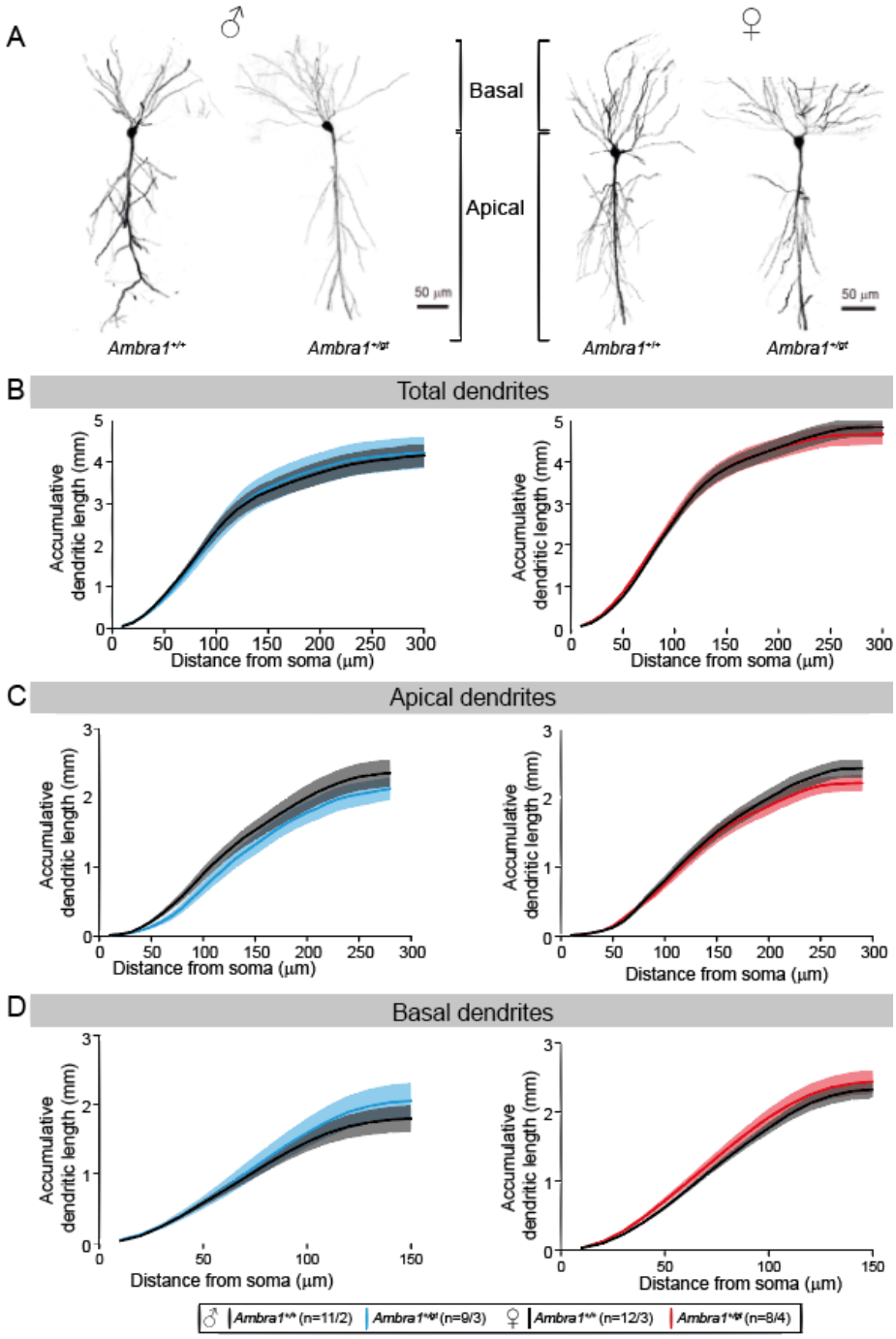

982

983 **Supplementary Figure S2: Sholl analysis from *in utero* electroporated neurons**

984 Data from male and female mice are placed on the left and right side, respectively. **A**
985 Representative picture of CA1 pyramidal neurons in hippocampus of *Ambra1*$^{+/+}$ and *Ambra1*$^{+/gt}$
986 mice in males and females at P28. **B-D** Comparison of dendritic length in whole (B), apical (**C**)
987 and basal (**D**) parts of pyramidal neurons in every 10 µm between genotypes in male and
988 female, separately. Neuron number/animal number are written next to the legends. Mean ±
989 S.E.M. are presented in line and area and statistical difference was defined by p-value between
990 genotypes from Repeated-Measures of ANOVA.

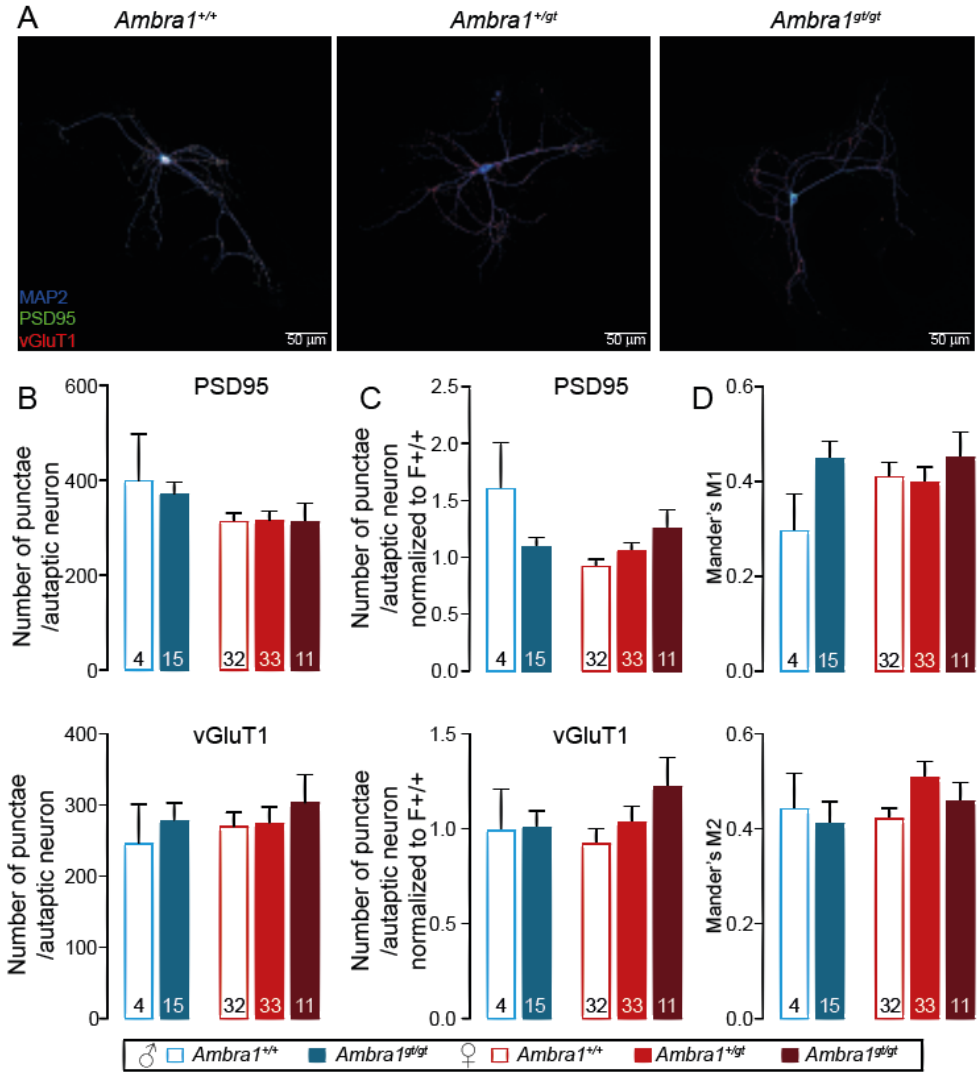

Supplementary Figure S3: Quantification of synapse number in glutamatergic autaptic hippocampal neurons

A Representative images of glutamatergic autaptic neurons from *Ambra1*$^{+/+}$, *Ambra1*$^{+/gt}$ and *Ambra1*$^{gt/gt}$ of E14.5 female hippocampi-like structures stained with antibodies against vGluT1, PSD95 and MAP2 at DIV18-23. **B, C** The absolute (**B**) or normalized number (**C**) of pre- (vGluT1-positive, above) or post-synaptic (PSD95-positive, below) puncta are shown. The normalization was done by dividing the average value of female *Ambra1*$^{+/+}$ cultured on the same day. **d** M1 (above) and M2 (below) coefficient of Mander's overlapping analysis between vGluT1 and PSD95 signals. The bar graphs represent mean ± S.E.M and the numbers of analyzed neurons are written inside the bottom of each bar. Statistical analysis between genotypes were carried out by two-way ANOVA followed by post-hoc Bonferroni test with significance level $p < 0.05$.